UTILIZATION OF COLD SPRAYING TECHNIQUE TO DEVELOP NI BASED COMPOSITES REINFORCED WITH NI_3AL PARTICULATES

A Thesis
Submitted to the Graduate Faculty
of the
North Dakota State University
of Agriculture and Applied Science

By

Tharaka Samudra Chandanayaka

In Partial Fulfillment of the Requirements
for the Degree of
MASTER OF SCIENCE

Major Department:
Mechanical Engineering

April 2015

Fargo, North Dakota

North Dakota State University
Graduate School

Title

Utilization of Cold Spraying Technique to Develop Ni Based Composites Reinforced with Ni_3Al Particulates

By

Tharaka Samudra Chandanayaka

The Supervisory Committee certifies that this ***disquisition*** complies with North Dakota State University's regulations and meets the accepted standards for the degree of

MASTER OF SCIENCE

SUPERVISORY COMMITTEE:

Dr. Fardad Azarmi
Chair

Dr. Dilpreet Bajwa

Dr. Val Marinov

Dr. Yechun Wang

Approved:

04/15/2015
Date

Dr. Alan Kallmeyer
Department Chair

ABSTRACT

This study was intended to investigate the capability of cold spraying deposition process as a near net shape forming technique to produce MMCs. P/M technique was used to fabricate MMCs in this study for the reason of comparison. Ni-Ni_3Al MMCs were fabricated using 80 Vol. % Ni and 20 Vol. % Ni_3Al using both methods. Microstructural characterization were conducted on all samples and powders. All fabricated samples were subjected to variety of experimental tests to determine mechanical properties. Observations of the microstructure of cold sprayed and P/M samples clearly indicated strong bonding between cold sprayed samples due to the low amount of porosity. Cold sprayed samples exhibited better mechanical properties compared to P/M samples. Reinforced samples showed slightly better mechanical properties compared to pure Ni samples regardless of the fabrication technique. Overall cold sprayed sample exhibited higher strength and denser microstructure with less porosity compared to the P/M samples.

ACKNOWLEDGEMENTS

I am taking this opportunity to express my gratitude to everyone who supported me throughout the Master's program. I am very grateful to Dr. Azarmi for giving me this invaluable opportunity to become a graduate student in the Mechanical Engineering department at NDSU and giving me constructive criticism and advice during the project. Apart from that I would like to acknowledge the Mechanical Engineering department, NDSU Electron Microscopy Center and Center for Nanoscale Science and Engineering for all their support and providing lab equipment and infrastructure. Special thanks to Mrs. Ajantha de Alwis for the great support. Finally I would like to thank my parents and my wife who has encouraged me to finish my master's degree in Mechanical Engineering.

DEDICATION

To My Mother - Priyani Jayakody

TABLE OF CONTENTS

LIST OF TABLES

LIST OF FIGURES

CHAPTER 1. INTRODUCTION

Nickel and its alloys are considered to be extremely valuable engineering materials due to their ability to withstand a variety of severe operation conditions which involve high temperature, corrosive environment, high stress, and sometimes a combination of all these harsh conditions. There are some explanations for outstanding characteristics of Ni and Ni based alloys. Ni possesses face center cubic (fcc) crystal structure with γ and γ′ phases present with ordered and disordered phase arrangements providing strength to the material at elevated temperature which naturally exhibit high toughness and ductility **[1][2]**

Nickel has excellent corrosion resistance in fresh water and non-oxidizing acids under room temperature. Ni alloys has also shown good corrosion resistivity at elevated temperatures. **[1][3][4]**. Although casting is still the major method for production of Ni based components, the high melting temperature of around 1453 ^{o}C makes application of fabrication techniques which involve melting of Ni a difficult task. Production of Ni based materials using solid state techniques became an important target for industries.

Aerospace and automotive industries seek materials with high strength performance at elevated temperature. The operation conditions and the efficiency of application such as jet engines can be increased significantly by selecting proper materials such as Ni and Nickel based alloys with high temperature and mechanical properties. Intermetallic compounds of Ni such as NiAl, Ni_3Al have melting temperatures above 1500 ^{o}C and high stiffness due to the strong binding between adjacent atoms **[1]**. Most ordered intermetallic compounds generally possess relatively low atomic diffusivity and dislocation mobility that cause their high strength at elevated temperature. Ni based materials can be designed with variable enhanced performance by adding alloying elements or in a form of Ni based composites. Considering Ni as the matrix,

different types of compounds such as Al, Co, Ti and Cr can be added to make a Metal Matrix Composite to achieve high strength and thermo- mechanical properties **[5]**. The idea of mixing Ni with some Ni based intermetallics seems to be interesting regarding the similarity and minimum mismatch between atoms of such a mixture. The idea of making composite materials using a solid state technique seems advantageous and interesting.

MMC consists of metallic material reinforced with metals, alloys, or ceramic particulates or fibers. MMCs generally offer better mechanical properties compared to unreinforced metals and can be designed to provide many diverse mechanical behavioral patterns such as high wear resistance, thermal expansion, and, corrosion resistance. MMC are manufactured with wide variety of techniques, among them liquid state techniques such as casting, solid state techniques such as powder metallurgy and electroplating, and gaseous state such as physical vapor deposition (PVD) are among the conventional methods of fabricating MMCs [**4**]. In addition, cold spraying has also been used to deposit MMC coatings **[1][5][6]**The cold spraying technique is a rapid deposition method that is mainly used to apply a protective metallic coating layer on the surface of industrial components. Generally, cold sprayed components exhibit high strength and high hardness due to low porosity content and a high degree of work hardening **[5]**. Cold spraying can be categorized as a solid state processing technique since it deposits particles on a substrate using supersonic velocity impaction below the melting temperature of the materials. Due to its unique method of spraying particles in the solid condition many problems phase change and oxidation associated with melting and solidification is eliminated in cold spraying **[7]**. Components manufactured by cold spraying also exhibit no build up thermal stress due to deposition below melting point **[7][8]**.

Powder Metallurgy (P/M) is a process that has been used for many years in human civilization, which is now firmly established in so many commercialized processes and industries. The basic concept of this technique is mixing and pressing powders to form a desired shape. The advantage of P/M technique compared to many other forming methods is that in general; there is no melting involved in the P/M process which reduces the phase change and formation of unwanted phases in the produced MMCs **[3]**. In the case of manufacturing the MMCs, P/M technique provides uniform distribution of reinforced powder among the matrix with less degradation resulting in isotropic properties **[3][8]**.

Even though the cold spray has been used in the industry for few decades there are potential commercial applications in the current market. Applications such as; refurbishment of aerospace parts using aluminum alloys, corrosion protective coatings for automobile and jet engines and heat sink can utilize cold spray technology. In addition, cold spraying technology is been used to produce coatings to increase corrosion resistance of sensitive materials using magnesium and aluminum alloys, braze joint preparation coatings, sputtering targets, chrome replacement coatings by deposition of WC-Co, and electrical and thermal conductive coatings [**7][8]**. Germany released the world's first mass production application of the cold sprayed components. This application is based on cold sprayed copper coating heat sink which is act as a thermal layer for both electronics and automotive parts **[10]**. Cold spraying itself presents an advantage on producing these coatings since it's reduce few fabrication steps compared to the conventional fabrications methods.

There are extensive amount of research have been performed in the area of P/M processed Ni based materials due to the simplicity of the manufacturing process and the greater performance. Cold spraying is relatively newer technology used in the industry compared to

P/M technique. Hence, there are not much research been done specifically towards Ni based cold spray coatings. However, with increasing demand of turbine parts that have higher service life and efficiency with temperatures beyond 800 ^{0}C, new materials are needed to be introduced **[2][9]**. Ni based alloys and MMCs are two such materials that have been introduced to these industries since Ni based materials have shown excellent properties under high temperature conditions such as creep resistance, corrosion resistance and strength **[1][14]**. The comparison between the two techniques in this study could potentially benefit to more effective implementation of cold spraying technique to produce Ni based alloys and composites and optimize the process parameters to increase the final quality.

The main objective of this study was to identify the effectiveness of cold spray technique as a manufacturing method to fabricate nickel based MMCs. In order to show the effectiveness of this technique, similar materials were fabricated using powder metallurgy process for the reason of comparison. The properties of fabricated MMCs by these two techniques were then compared to the ones obtained from samples of un-reinforced pure Ni produced by similar techniques. The objectives of this study can be summarized as:

1. Study the effect of adding Ni intermetallic reinforcements to the Ni matrix via mechanical and microstructural characterization.
2. Investigation on the effect of particle size of reinforcement phase on the mechanical properties of the cold sprayed and P/M processed Ni-Ni_3Al composites. Two different particle sizes of reinforcement (Ni_3Al) were used and the matrix particle size was kept constant for both composites.
3. The microstructural and mechanical properties of un-reinforced and reinforced cold sprayed samples were compared to those from P/M technique to understand the

effectiveness of cold spraying technique in production of Ni based composites as a solid state technique.

4. The effect of heat treatment on the microstructural and mechanical properties of un-reinforced and reinforced samples fabricated by both techniques were also studied in this research.

In order to attain the above mentions objectives, various testing methods were performed on the fabricated samples. The microstructural characterization was conducted using optical, scanning electron microscopy and Energy dispersive spectroscopy methods. Then the image analysis and density test were performed on the all the samples to evaluate the different phases and to understand the porosity content. The mechanical characterization was mainly based on elastic modulus and the hardness properties. Elastic modulus was measured since it provides overall information in materials. The defining of elastic modulus on coating materials cannot be achieved using a conventional process such as tensile testing due to inhomogeneity and very low thickness of these materials. The elastic modulus of the sprayed coatings and P/M samples were obtained using Knoop indentation testing and some available analytical models, and the values were validated with the resonance frequency testing and nano-indentation test. Vickers test was performed to validate the hardness results obtained from Knoop test.

CHAPTER 2. LITERATURE REVIEW

2.1. Introduction

High performance materials have become very critical in modern aviation and aerospace which is directed towards turbines and engines. Jet engines are manufactured with reinforced materials to enhance the mechanical properties and the operational life of the parts, which is directly correlated to the performance and the efficiency of the overall engine. Mostly jet engines and gas turbines are manufactured with materials that can withstand very high temperatures while generating power under the harsh operational conditions **[2][11][12][13][15]**. Materials such as Titanium seems to be suitable candidate with lower weight concern, however with high temperature conditions, the oxidation parameters needed to be taken to the account. Hence the Ti has lower oxidation resistance under high temperature conditions, it is not suitable for being used in many sections of jet engines and gas turbines that are operated above 700 ^{0}C **[2][15][16]**. Ferrite steel is another material that is used in manufacturing of the components for service in high temperature environments such as inducing nuclear reactors and turbine blades. It exhibits very good creep resistance at temperatures up to 750 ^{0}C **[11] [16]**. Nickel and Nickel based alloys seems to be the one of the best suitable materials for high temperature application. Following more information regarding nickel and its properties in provided.

2.2. Nickel and Nickel Based Materials

Ni is one of the very important and versatile materials in the metal industry. Bulk Ni illustrates high melting temperature, tensile, electrical and magnetic properties. Ni is known as one among three elements apart from iron and cobalt exhibiting strong ferromagnetic properties at room temperature **[14][17]**. Ni is being widely used as an important alloying element in

production of ferritic alloys, cast iron and steel. Due to high melting temperature of Ni which is approximately around 1453 ^{o}C, Ni and its alloys have been used in many high temperature application, where majority of those applications involved heat and corrosion resistance at elevated temperatures. Table 2.1 lists the industries and the particular applications/parts of Ni **[14]**.

Table 2.1. Applications of Ni and Ni based material.

Industry	Application /parts
Aircraft gas turbines	Disk, combustion chambers, exhaust systems, blades after burners
Metal processing	Hot work dies and tools
Automotive industry	Catalytic converters, spark plugs
Coal	Piping , heat exchangers
Aerospace	Heat sinks, Rocket engine parts
Steam turbines	Blades, bolts
Petroleum	Fans, values, reaction vessels

Ni based composite can be designed with variable enhanced performances by adding reinforcement phases. Xu et.al (1997) reported well-known technique to improve the brittle behavior of Ni compounds by addition of small amount of Boron **[5]**. Considering Ni as the matrix, different types of compounds such as Al, Co, Ti and Cr can be added to make Metal Matrix Composites to achieve high strength and improved thermo- mechanical properties **[6]**.

Nickel based alloys are recognized as one of the most effective materials with unique properties such as, higher toughness, resistance to corrosive conditions and higher flexural strength under high temperature environments. In addition, Ni based materials are used in oxidizing conditions because of its higher resistance for degradation **[1][3]**. Aviation industry has shown a keen interest towards Ni based materials due to the excellent characteristics as mentioned. Rocket engines, turbines and nuclear and chemical plants widely use Ni based materials **[15]**.

Alloys that are used in high temperature conditions can usually service tolerate up to 1100 ^{o}C-1200^{o}C **[2][6][14][17]**. Most of the metals that are used in the industry have melting points lower than 1200 ^{o}C. This underlies the importance of Ni based materials that melt at higher temperatures. Aircraft engines are usually manufactured with Ni based material that composes 40-50% by weight of the engine **[16]**. Ni based materials are used towards the combustor and the turbine section where the highest temperature is achieved in the engine at operation conditions. Different types of the forming methods have been used to fabricate the turbine and engine parts. Investment casting technique is used to fabricate complex and variable shapes of turbine blades and structural components in engines. In investment casting cooling cycles can be altered to control the grain structure of the blades. Since these parts are operated at high temperatures, it is critical to eliminate the grain boundaries as much as possible. Since, lower number of grain boundary sites provides less damage from the heat accumulation due to less surface area formation from the lower grain boundary sites **[2]**. Grain boundaries can be minimized by using single crystal casting **[16]**.Wrought processing is commonly used to fabricate the turbine disk to acquire resistance to crack growth, greater strength and toughness

[2][16][17][18]. These exceptional properties can be reached in Ni based materials using several stages of controlled wrought processing.

Nickel based alloys and composites are primarily combined with Ti, Co, Cr and Al due to their unique properties. Apart from that, small quantities of Boron and Carbon can be added to Ni that makes the complex bonding structure due to 4d and 5d orbitals **[16]**. The outer shell been S and P orbitals in Boron and Carbon respectively compared to the 4d and 5d orbitals in Ni. Due to the different orientation of the arrangement of these three elements, it will create a complex bonding structure at the equilibrium. Atomic radius is a critical factor for the alloying elements of Ni. Co and Cr has similar radius compared to Ni that will come to equilibrium with gamma (γ) phase. Al and Ti has larger atomic radius compared to Ni, where the equilibrium will occur by creating a gamma prime (γ') phase **[18]**.

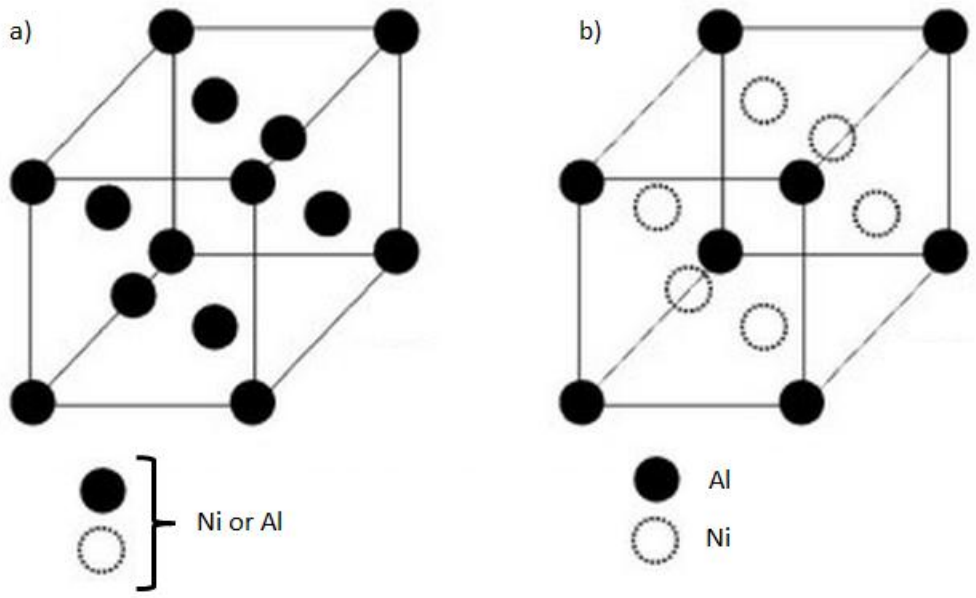

Figure 2.1. Crystal structure of (a) Gamma (b) Gamma prime containing Ni and Al as elements.

Figure 2.1(a) shows the γ phase with face center cubic (FCC) crystal structure which has a disordered phase and creates the matrix of alloys. Figure 2.1(b) shows the γ′ phase which has a $L1_2$ ordered structure. Gamma phase is generally soft compared to γ′ phase where [100] plane of γ phase tend to convert in to γ′ phase by elastically softening **[19]**. One of the significant characteristics of γ′ phase is that it provides strength to the material at elevated temperature **[19]**. The nickel aluminide intermetallics have been studied extensively because of their excellent high temperature mechanical properties. Most of these studies have focused on the controlling fracture and deformation mechanisms of single and polycrystalline Ni-Al combinations in association to their potential application as a high temperature "superalloy" for aerospace applications. Figure 2.2 shows the Ni-Al binary phase diagram. When the amount of Al increases in to a Ni- Al binary system, another phase forms as a precipitate that has γ′ structure. Different intermetallic components can be created at different compositions such as NiAl, Ni_2Al_3 and Ni_3Al, etc.

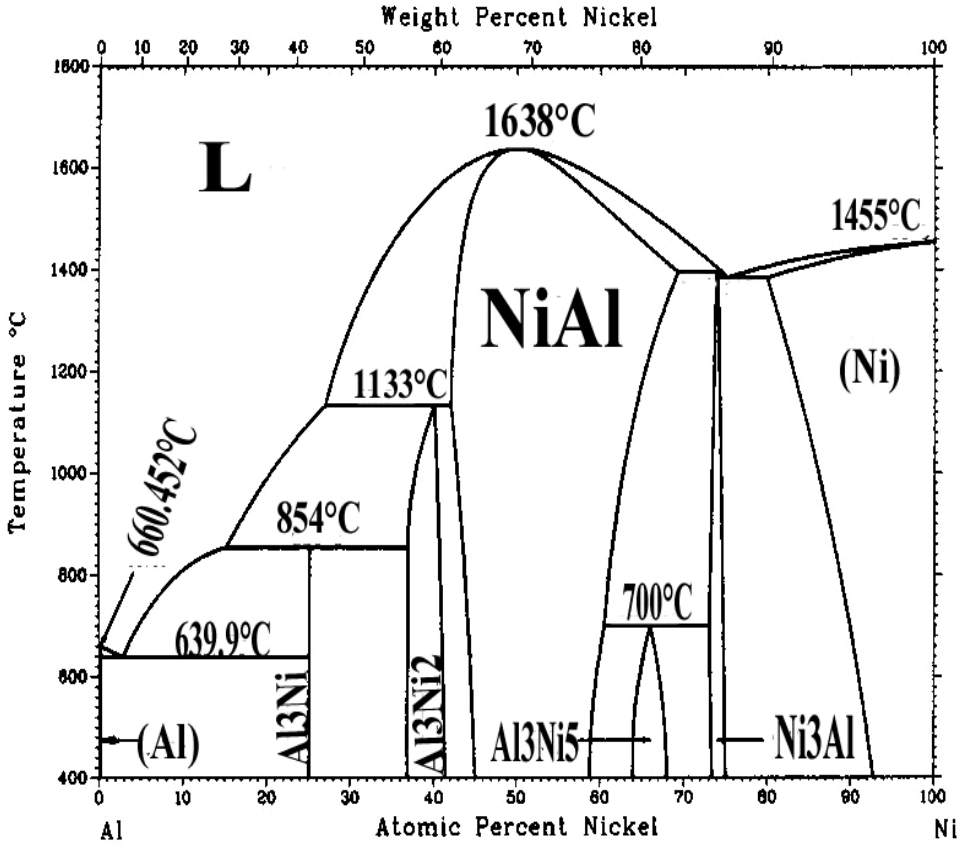

Figure 2.2. Phase diagram of Ni-Al [**20**].

With addition of Al (13-15% vol.) into Ni (85-87% vol.) and once it reaches the equilibrium level, the Ni_3Al intermetallic will form which has an ordered FCC structure with γ′ phase. Both γ′ and γ phases are sensitive to the cooling rate, where slow cooling rate promotes γ precipitates around 40 K/min **[18][19][20][21]**, whereas, the higher cooling rate tends to create γ′ precipitates **[19]**. Many studies have been conducted to observe the cooling rate effect on the microstructure and the mechanical properties of Ni based materials. Sajjadi et.al (2008) studied the effect of cooling rate on Ni based alloy UDIMET 500 that are used in second stage of high powered gas turbines **[22]**. UDIMET has a combination of Ni, Cr, Co, Ti, Al, Mo, Fe and C in fallowing weight representing 48.69%, 17.9%, 17.2%, 3%, 3%. 4%, 2.1% and 0.11%,

respectively. Experimental results of this study have shown that increase in cooling rate has increased the tensile strength and yield straight. Mao et.al (2002) have studied the effect of γ′ phase on cooling precipitation and strengthening of Rene88DT manufactured using P/M method. The results indicated that there is a power low relationship between the rate of cooling and the size of the γ′ precipitates **[23]**.

The microstructure of Ni consists of Ni -γ precipitate and adding Ni_3Al will add fully ordered γ' which depresses with γ disordered precipitate to increase the strength and toughness of the MMC by added dislocations and age hardening **[20][21][22][23]**. The basic phenomenon of the strengthening mechanism of metals is by minimizing the mobility of dislocations by reducing the occurrence of plastic deformation. Particle reinforcement phase will act as an obstacle for dislocation motion in MMCs. The oldest method for the fabrication of metal matrix composites is the solid-state process. This study uses solid state technique via two different processes to fabricate required samples. The first method is the cold spraying, and the second method is powder metallurgy (P/M) technique. The detail of each technique is explained in the next sections.

2.3. Cold Spraying Process

Plastically deformed metal particles either by means of higher velocity, molten, or combination of both can be deposited in a substrate to form a coating **[14]**. This can be achieved by the most of the thermal spraying processes where molten, semi-molten or solid particles are deposited on a substrate. Cold spray technique also known as Cold Gas Dynamic Spraying Method (CGSM) is categorized under thermal spraying techniques where the major difference is that here the sprayed particles are deposited in solid state condition **[24][25]**.

Cold spraying deposition system has been used by few industries to apply protective layers on the surface of components to enhance their wear and corrosion resistance **[8][26][27]**. One of the unique characteristics of this process is the capability of manufacturing high purity metal coatings with highly improved properties compared to the usual cold worked processed parts and components **[8]**. Cold spraying technique offers several outstanding characteristics such as; low residual stress, less heat input towards substrate, higher deposition efficiency and compositional stability **[27]**. This technology mainly used in aerospace, automotive and gas turbine industry **[1][8][10][28]**. Apart from that cold spraying is capable of fabricating near net shapes components and can also be used for repairing of damaged surfaces **[27]**. Cold spraying can be used to fabricate near net shape parts with variable composition by controlling the feedstock with the aid of programmable robot gun. Figure 2.3 shows the near net shape parts that has been fabricated using cold spraying technique **[28]**. Thin and thick layers of thermal barrier coatings can be deposited using cold spraying technique. This technique can also be used for deposition of coatings to mitigate the radiation and corrosion damages used in aerospace application **[10][27]**.

Figure 2.3. Near net shape parts fabricated using cold spray technique **[10]**.

Since the particles are sprayed at solid condition, this process is limited to ductile and deformable materials. The brittle particles will shattered when hit the substrate at high velocity during cold spraying. The comparison of cold spraying vs other thermal spraying in terms of temperature and particle velocity is illustrated in Figure 2.4.

Cold spraying system contains a diverging/converging nozzle where the accelerated particles are sprayed in to a substrate with velocities in the range of 300-1200 m/s. The substrate is generally located 25-30 mm from the nozzle. Supersonics gas jet is used to accelerate particles at a temperature below the melting point of the particles. The particles with high kinetic energy will plastically deform on the substrate during the impact forming splats. Deposition of

thousands of splats on top of each other, which are bonded together, forms the final coating structure. This process comprising low temperatures avoids many deficiencies in other thermal spraying methods such as melting, crystallization, high temperature oxidation and thermally induced residual stresses **[24][25][28]**.

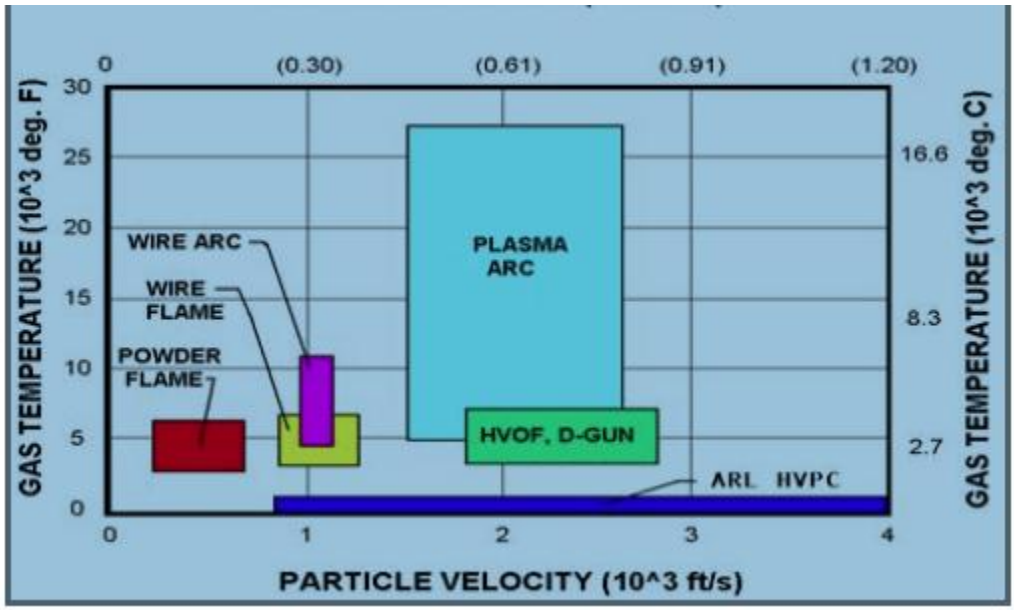

Figure 2.4. Comparison of Cold spraying technique respect to process temperature and particle velocity of other thermal spraying methods **[8]**.

Two different types of cold spraying systems have been developed according to the carrier gas pressure. The low pressure Cold spraying system (LPCS) utilizes lower pressure of 5-10 bars while high pressure cold spray system (HPCS) uses gases at the pressure of 25-30 bars [**10**]**[25][28][29]**. Beside the pressure difference among these methods, LPCS uses radial injection where the powder feeder is introduced radially to the downstream of the supersonic nozzle. HPCS uses axial injection where the powder is introduced axially towards the downstream.

LPCS uses maximum of preheating temperature up to 550 ^{0}C to reduce the moisture content and increase the aerodynamics properties of the flight while deposition. Due to the lower pressure, the heated gas can reach up to 300- 600 m/s speed. Thus, the LPCS is only capable of depositing soft ductile metals such as Cu and Al. Apart from the that, there are a few advantages on using the low pressure systems, such as low overall cost due to the nitrogen and air being used as the career gas, low maintenance and wear, longer service life, and this system can be easily modified due to less complexity **[29][30]**. However, when using the low pressure and the lower acceleration on career gas, the efficiency of the LPCS is around 50%. The efficiency is a measure of the bonding and deposition rate or particles to the substrate. Due to lower kinetic energy absorbed by the particles, it tends to bounce back from the substrate hence the efficiency could reduce up to 50%.

The HPCS uses the preheating temperature up to 1000 ^{0}C to increase the aerodynamic properties. In addition, the HPCS is capable of using less ductile metals such as Ni, where higher preheating temperatures will soften the particles slightly prior to the deposition. With higher pressures, the preheated gas accelerates the powder particles up to 1200 m/s speed which provides the spraying efficiency around 90% **[24][29]**. This will induce better mechanical bonding in the coatings. The difference in the LPCS and HPCS is shown in Figure 2.5 and Figure 2.6.

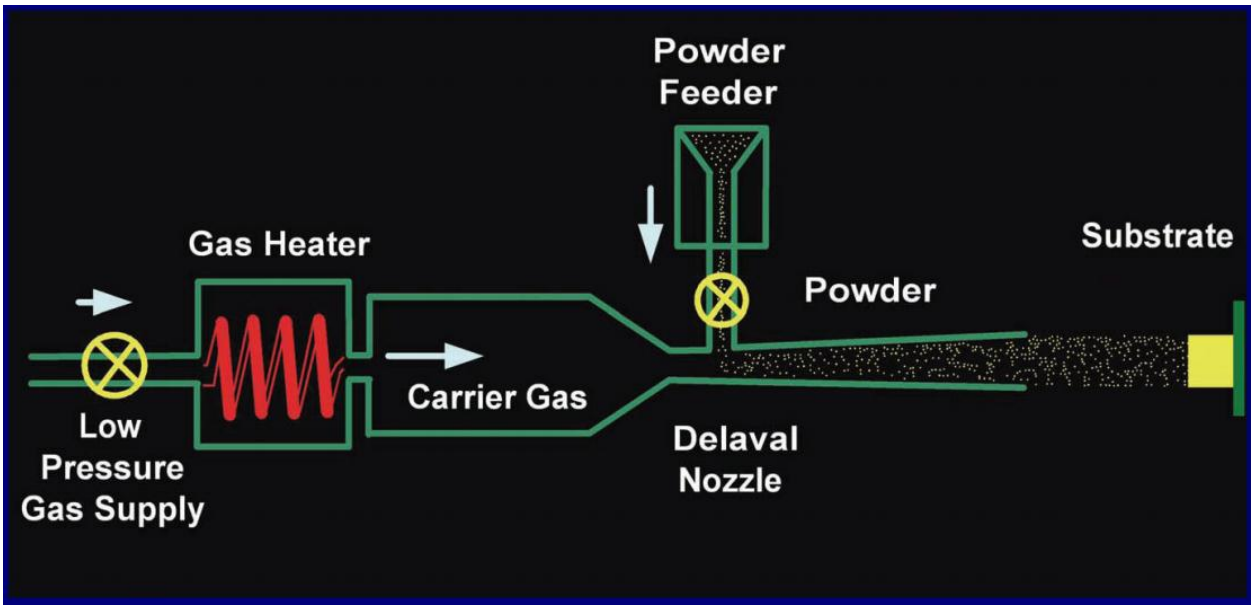

Figure 2.5. Schematics of low pressure cold spraying system (LPCS) **[25]**.

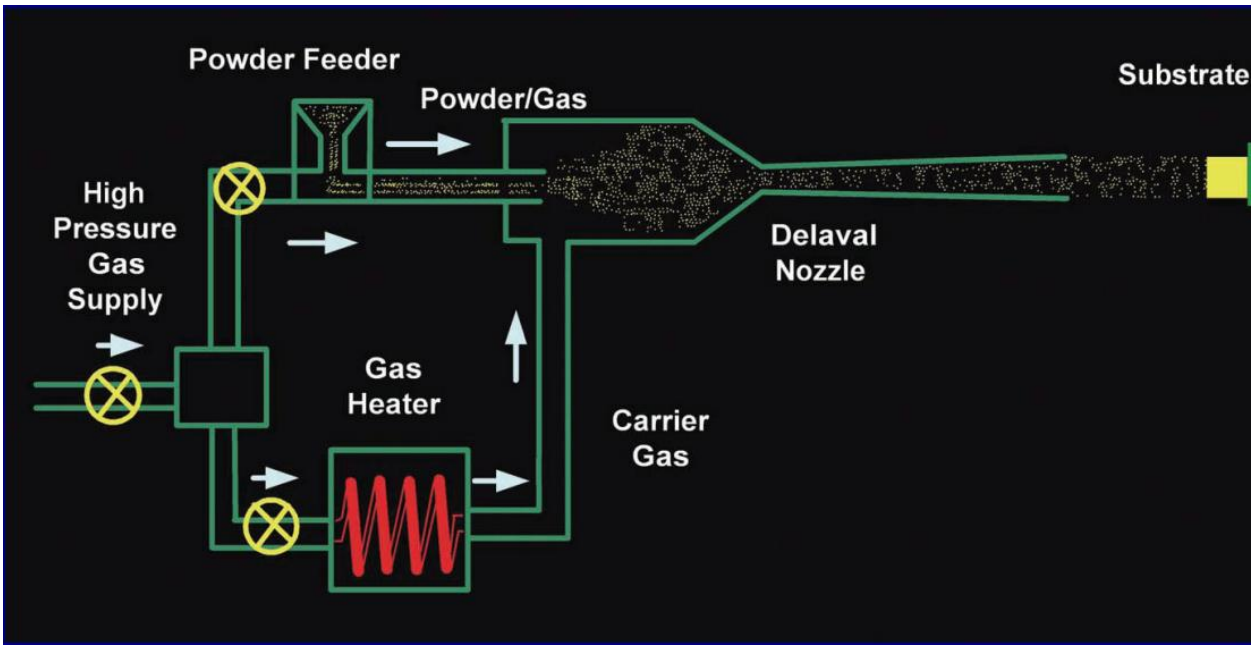

Figure 2.6. Schematics of high pressure cold spraying system (HPCS) **[25]**.

2.3.1. Spraying Parameters

There are several operational parameters which influence microstructural and mechanical properties of cold sprayed coatings. Spraying parameters such as pressure, standoff distance, and particle temperature will define impact velocity, deposition efficiency which consequently influences coating strength and its adhesion to the substrate. In addition operating gases, powder feed rate, and particle size can be named as a few other spraying parameter in a cold praying system. Standoff distance and the pressure can be varied depending on the low pressure and high pressure cold spraying systems. High pressure is obtained using higher compressed gas for spraying particles.

Legoux et al. (2007) has studied the change in substrate temperature using an infrared camera during the process of deposition **[31]**. The coatings formation was closely investigated as a function of particle velocity and surface temperature of the substrate. Legoux results showed higher deposition rates at higher substrate temperatures. Cold spraying been a low temperature thermal spraying process that relies mostly on plastic deformation to produce low porosity coatings, there are many aspects of particle adhesion and impaction need to be researched. Finite element modeling has been incorporated with experimental results from cold spraying particle impact to develop three dimensional models to understand the several deposition parameters **[32]**. Li et al. (2009) studied the behavior of Cu particles impaction using cold spraying technique with aid of 3-D modeling **[32]**. Li has observed that the particle size variation has slight effect on the morphology of the coatings. Particle size is a critical spraying parameter that studied further in this study which discuss in-depth in chapter 4.

In order to manufacture coatings with the desired microstructure, the relations between particle characteristics and the spraying parameters need to be fully understood. Then, the

relation between the microstructure of the coating and the characteristics of the particles can be established.

Due to the high velocity involved in the cold spraying process, any small changes in the spraying parameters may result in significant changes in the in-flight particle characteristics and thus in the final properties of the coating.

Type of the nozzle defines velocity and system pressure and selection of optimum nozzle requires close attention which consequently influence the deposition quality of the particles in clod spraying process. The velocity of in-flight particles is directly controlled by the spraying process parameters. Some studies have described the correlations between operational spraying parameters, and particle velocity **[30][33][34]**. The critical velocity determined the effects of impinging particles changes from erosion to deposition on the surface of the substrate. Critical velocity is a variable factor that based on many factors such as the substrate, particle material, surface condition, spray angle and particle size **[32][33]**. However the velocity of particles itself depend on the geometry of the nozzle, operating temperature and pressure of the system **[33] [34] [35] [36]**.

2.3.2. Mechanism of Splat Formation during Cold Spraying Process

There are a several studies that have been done to understand the mechanism of splat formation during cold spraying deposition. Since the gas temperature in cold spraying is much below the melting temperature of particles bonding mechanism can be predominantly caused by plastically deformation of particles on targeted surface **[30][36]**. However the preheated particles always carry higher kinetic energy that strengthen splat due to thermal softening.

Champagne at el. (2005) proposed a ballistic model and theory to explain the bonding mechanism of Cu particles on Al substrate using cold spraying method **[37]**. Figure 2.7

demonstrate the four different steps of the deformation that takes place when a spherical copper particle is impacted on an aluminum substrate **[37]**. The deformation mechanism shown in this figure indicated that the interface has been acting like a viscous fluid which shaped as a wave and rolled-up to enhance the bonding properties **[37]**. Figure 2.8 shows the SEM image of Cu coating (Light gray) on Al substrate (dark gray).

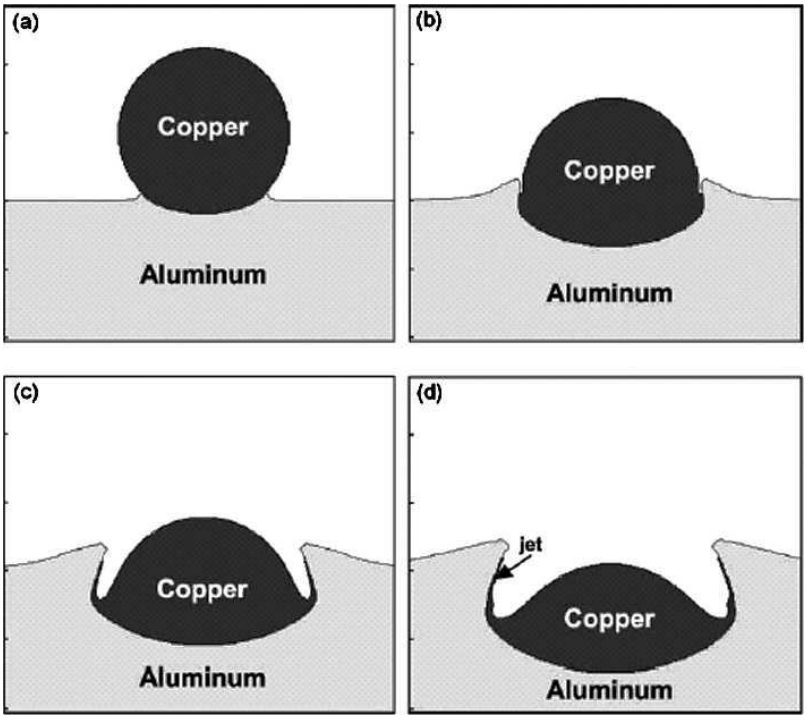

Figure 2.7. Simulation of impaction of a Cu particle on a Al substrate at successive intervals of : (a) 5 ns, (b) 20 ns, (c) 35 ns, and (d) 50 ns **[37]**.

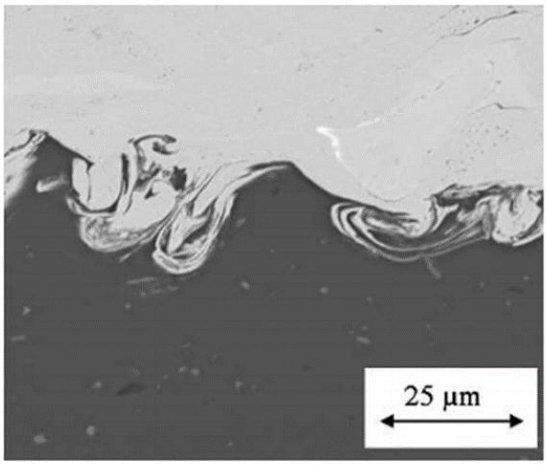

Figure 2.8. SEM image of cold sprayed Cu on Al substrate **[37]**.

2.4. Powder Metallurgy

There is a high demand for simple and cost effective techniques which can produce parts and components with relatively high quality. Since, powder metallurgy (P/M) has the capability of mass production of components with simple geometry at a lower cost with less machining with advantages over many other forming processes **[38]**. P/M can be defined as a process that fabricates components and parts using raw metal powders or mixture of powders using softening compaction of particles followed by heat treatment. .

The P/M technique has the following advantages over other fabrication techniques for MMCs. The mechanical strength of composites made by the P/M technique are generally better than those made by liquid metal techniques. This is because the P/M technique results in more uniform distributions of the reinforcement phase. Although the P/M technique is prone to void formations in the material due to incomplete bonding, the microstructure of properly made P/M composites has fewer defects than cast composites because it is free of porosity associated with solidification.

What follows is a detailed description of the steps in the P/M fabrication process, which has outlined in Figure 2.9 This description will cover information that is directly relevant to the fabrication of MMCs in this study.

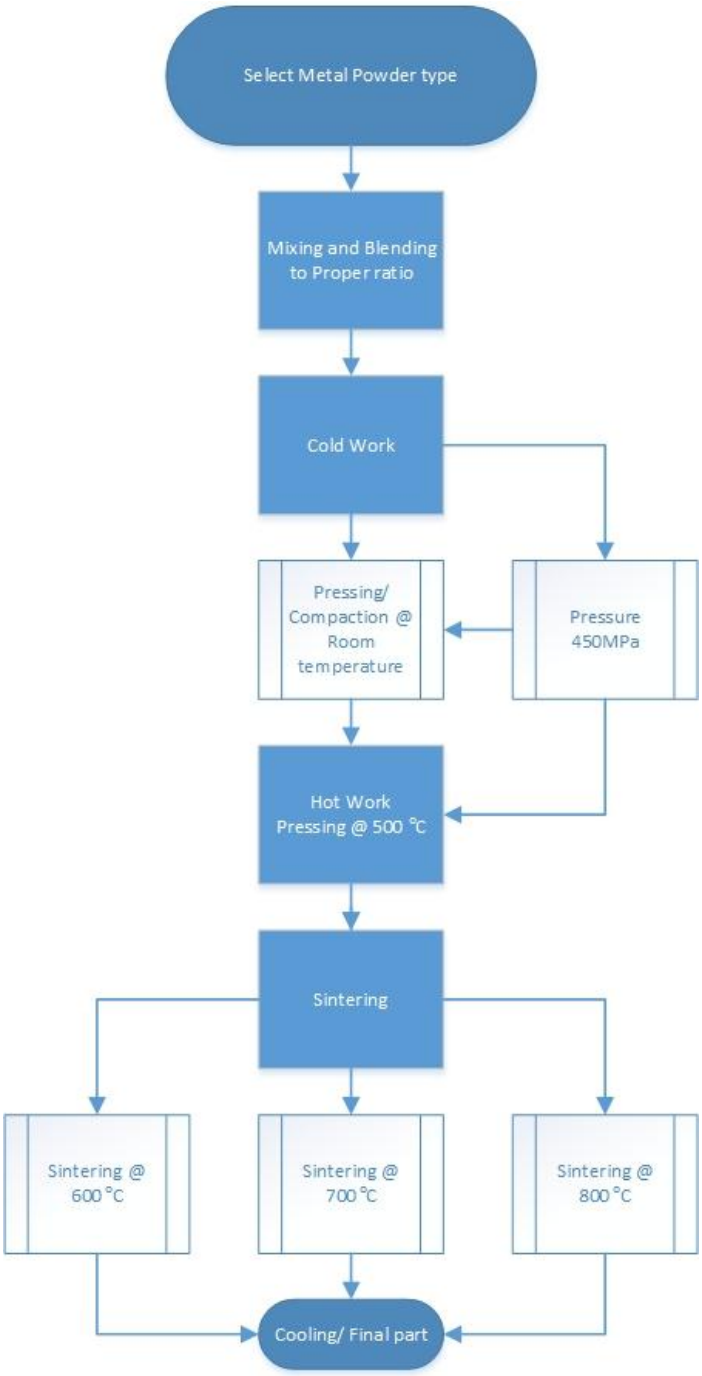

Figure 2.9. P/M technique process flow diagram.

2.4.1. Mixing and Blending

The fabrication of composites by the P/M technique requires complete mixing of the reinforcement and matrix powders. In addition, mixing pure metal powders with pure alloy elements is often preformed to create a metal alloy by solid-state inter-diffusion during the sintering and hot pressing stages. This results in a composite containing a metal alloy matrix. In this situation, uniform mixing of the metal and alloy powders is required in addition to uniform mixing of the metal with the reinforcement powders.

Incomplete mixing of the powders occurs from three causes: 1- Particle size differences between the metal powders and the reinforcing powders, 2- differences in density of the metal and reinforcement powders, and 3- irregular particle shapes causing inter-locking of particles and incomplete mixing **[39]**.

2.4.2. Cold Compaction

The cold pressing process is necessary to compress the powders into a state where sufficient contact occurs between the powders for significant inter-diffusion to occur during the sintering stage. Cold compaction is usually performed by isostatic pressing at room temperature; however the process can also be performed by rolling, die compacting, or injection molding.

2.4.3. Sintering

Compressed powders are normally subjected to a degassing and sintering treatment. This process helps to remove of trapped air and additives using in the mixing and blending stage and results to a semi ideal dense composite. Successful performance of this process also removes water vapor and gases absorbed to particles. Shrinkage (porosity decrease) may occur during sintering by rearrangement and center approach due to inter-diffusion of atoms that result in a

decrease of the internal surface area as it is shown in Figure 2.10. To obtain the best results, this process always performs in the inert gas Atmosphere or vacuum **[40]**.

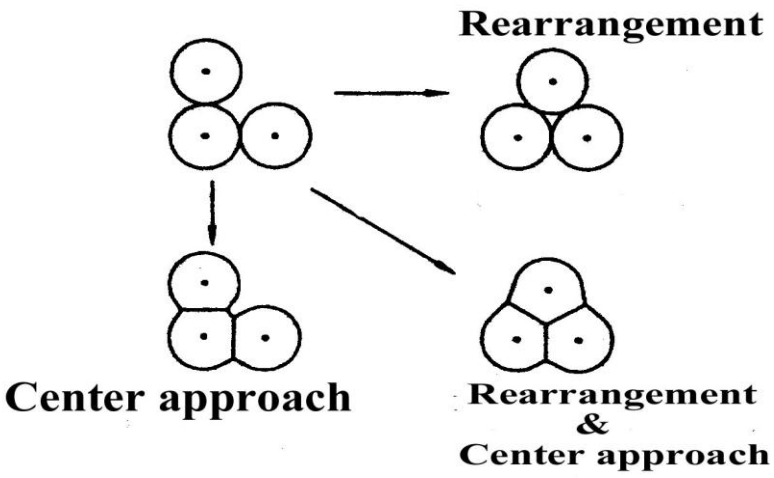

Figure 2.10. Shrinkage by rearrangement and center approach during sintering process **[40]**.

Three different stages of sintering process can be recognized in the Figure 2.9; first, the rearrangement stage when particles contact at a maximum ratio. Then, a necking forms between the particles due to the inter-diffusion. Finally, the geometry of particles will completely change accompany with a significant reduction in the pores numbers and shapes. Sintering time and the operational temperature are two important parameters defining the final characteristics of products **[41]**.

2.4.4. Consolidation

Hot isostatic pressing or extrusion can perform the hot pressing process. Hot isostatic pressing can be considered as the most effective route for consolidation of metal matrix composites with high volume fractions of reinforcement. Hot pressing applies for simple

geometries and the result is mostly consolidated to close to ideal density products. In addition, micro oxidation may occur during P/M fabrication process. A thin oxide layer may cover all the particle powders, which restricts the full contact of the particles resulting in decrease in inter-diffusion during sintering process. Application of pressing is not enough to satisfactory break these oxide layers. Applying an additional pressing at high temperature could break the oxide layer in small particles **[42]**.

There are several methods to manufacture required powders to be used in the P/M technique. Metal powders are produced by mechanical milling or chemically. The mechanical milling uses ball bearing or hammering methods to manufacture metal powder. In the chemical process, different types of chemical agents and compounds are used to reduce the metals. P/M technique is capable of using wide range of materials. In general, ductile metals are combined to manufacture alloy or reinforced can be added to manufacture composites. Lubricants are also added to this process as a binder such as paraffin wax, to make better mechanical bonding prior to sintering.

Most of the components manufactured using the P/M contains porosity mostly up to 15% **[38][43]**. In general these components are exposed to very high stresses; hence the capacity of enduring these higher loads can be enhanced by hardening process. However to manufacture a high quality parts using the P/M, it is crucial to distribute the porosity homogenously within the microstructure **[43][44]**. In addition the porosity can act as a crack initiation site that will reduce the strength and the service life of the P/M parts depending on the loading condition, temperature, surrounding condition **[38]**.

Special attention has been made to P/M parts service under high temperature applications such as turbine engines, manufactured with Ni based materials. With the high temperature

involved with structural components, fatigue crack growth needs to be studied since it could fail the parts catastrophically. Solomon et.al (1973) and James at.al (1976) investigate on the environmental effects on the parts that are fabricated from the P/M. Solomon point out that oxidation due to environmental exposure could lead to increase in rate of fatigue crack growth **[45][46]**. Yang et al. (2011) has studies the crack growth behavior of nickel based P/M parts at R.T, 550 ^{0}C, 650 ^{0}C respectively. They proposed that, with higher temperature, creep damage induce on the P/M parts due to the grain boundary weakening increases the crack growth **[47]**.

2.5. Metal Matrix Composites (MMC)

Metal matrix composites (MMC) were developed over the last seventy years. They exhibit unique microstructures and characteristics which are not found in conventional monolithic metals or ceramics **[48]**. A composite material can be defined as a material that usually consists of two or more physically/chemical distinct phases. The reinforcement material generally distributed within the structure, and when the matrix is metallic material; it is called as metal matrix composite **[49]**. There are verity of material that can take the form of reinforcement such as; particles, short or continuous fibers and whiskers **[49]**.

Mechanical properties of MMCs directly correlated to the matrix and reinforcement materials, distribution of reinforcing phase, size and shape of reinforcement materials and the interfacial bonding between reinforcement and the matrix **[50]**. MMCs can be manufactured with high dislocation density with limited recrystallization resulting in superior mechanical properties [**51**]**[52][53]**. There are few fabrication methods that use in to industry to produce MMCs. Casting, diffusion bonding, powder processing and deposition techniques are some of these methods **[50][51]**. Castings can categorize under liquid state processing of MMCs that mix the two phases by means of melting. Diffusion bonding is a solid state process that takes place at

elevated temperatures to create bonding between dissimilar metals. Controlling the volume fraction and capability of processing wide verity of materials are the major advantages of using this technique. Powder processing is further discussed in section 2.4 in detail. Electroplating, chemical vapor deposition (CVD), physical vapor deposition (PVD) and thermal spraying are few deposition methods that used to fabricate MMCs **[48][54]**. Cold spraying which is used in this study will be discussed in details in section 2.3.

MMCs are still finding many applications in automotive, aerospace and electronics. Many studies were conducted to optimize the mechanical properties of MMCs. It is critical to acquire the optimal particle size to obtain the improved mechanical properties in MMCs. Prasad et al. (1995) studied the relationship between the Relative Particle Size (RPS) between the matrix and reinforcement particles manufactured with 2124 Al -SiC MMCs **[55]**. This study has shown that the mechanical properties such as ductility, and strength increased with the decrease in RPS **[55]**. On the contrary, Lewandowski et al. (1995) reported of an improvement in mechanical properties of aluminum based MMC with the increase in RPS **[56]**. The composite was fabricated from Al-7Zn-2Mg-2Cu-0.14Zr reinforced with 20 %Vol. SiC with size range of 5μm-16μm **[54][56][57]**. A similar study was conducted by Yoshmura et al. (1997) to find the relationship between the particle size and the mechanical properties of MMCs **[58]**. They have reported that there is no particular trend between the particle size and the mechanical properties. Jodoin et al. (2006) studied effect of particle size of Scandium (Sc) reinforcements with 2618(Al-Cu-Mg-Fe-Ni) aluminum alloy coating deposited using cold spraying technique **[59]**. Sc powders were deposited with two different particle sizes, one below 25 μm and the other one between 25 and 38 μm **[59]**. The smaller particles exhibited higher velocity compared to the larger particles. The higher velocity in the smaller particle can be attributed to the inverse

relationship between the diameter of the particles and its acceleration **[59]**. The smaller particles have produced less porous coatings and harder structure compared to the larger particles.

Thermo-mechanical properties of the MMCs are mainly based on their microstructure characteristics, morphology, and interfacial properties between splats. Some unwanted phases such as oxides, and voids would associate within the coating structure during the coating process **[60]**. Koivuluoto et al. (2015) studied the effect of heat treatments on Ni reinforced with 30% vol. Cu that is deposited by cold spraying method **[61]**. They reported that the cold sprayed Ni coating showed denser structure after heat treatment process Yang et al. (2008) studied the effect of phase transformation of cold sprayed Ni/Al-$Al2O_3$ coating with heat treatments **[62]**. According to this study during the heat treatment process, the coating has become denser which can be attributed to the diffusion mechanism on NiAl intermetallic compound. All these studies indicate the addition of reinforcements had benefited the mechanical properties or the microstructure of the MMCs.

CHAPTER 3. EXPERIMENTAL PROCEDURE

3.1. Overview

This chapter presents the procedure that was used to perform this investigation. Specific information about materials used in this study is mentioned in section 3.2. The processes used to fabricate the samples are discussed in Section 3.3. The microstructural characterization that was performed on these samples is described in Section 3.4. The mechanical tests, Knoop and Vickers micro-indentation tests, Nano-indentation, and Resonant Frequency test, which were performed on the samples, are described in Section 3.5.

3.2. Powder Preparation

Commercially available Ni powder with 99.5 wt. % purity (Centerline Limited, ON, Canada) with nominal particle sizes of >50 μm and <100 μm was used to fabricate cold spraying and P/M samples of pure nickel. Gas atomized Ni_3Al with nominal particle sizes of >5 μm and <45 μm with99.0 wt. % purity (Reade Advanced Materials, Riverside, RI, USA) were added and mixed with the pure nickel powders with a ratio of 80 vol. % of Ni and 20 vol. % of Ni_3Al for the fabrication of MMC samples. The samples were mixed using a high speed powder mixer for 5 minutes at room temperature.

3.3. Sample Fabrication

A total of 12 samples were fabricated from Ni and Ni-Ni_3Al materials using the cold spraying method and P/M method in this study (3 samples of each). In order to evaluate effect of the particle size, the two types of powder blends were created. The particle size distributions of

the two blends are shown in Table 1. Two different blends were used to fabricate samples using both cold spraying and P/M technique.

Table 3.1. Powder size variation of Blend I and II.

Material	Ni Nominal Particle size (80 vol. %) μm	Ni_3Al Nominal particle size (20 vol. %) μm
Blend I	>50 and <100	>5 and <45
Blend II	>50 and <100	>45 and <100

3.3.1. Cold Spraying

The pure Ni and premixed 80 vol. % of Ni and 20 vol. % of Ni_3Al powder was sprayed onto aluminum substrates in a size of 76.2mm L × 31.75mm W× 5.08mm T. Samples were manufactured by Centerline Limited, Windsor, ON, Canada using a high pressure SST-P Series cold spray system. Schematic of high pressure cold spray system (HPCS) used in this study is shown in Figure 3.1.

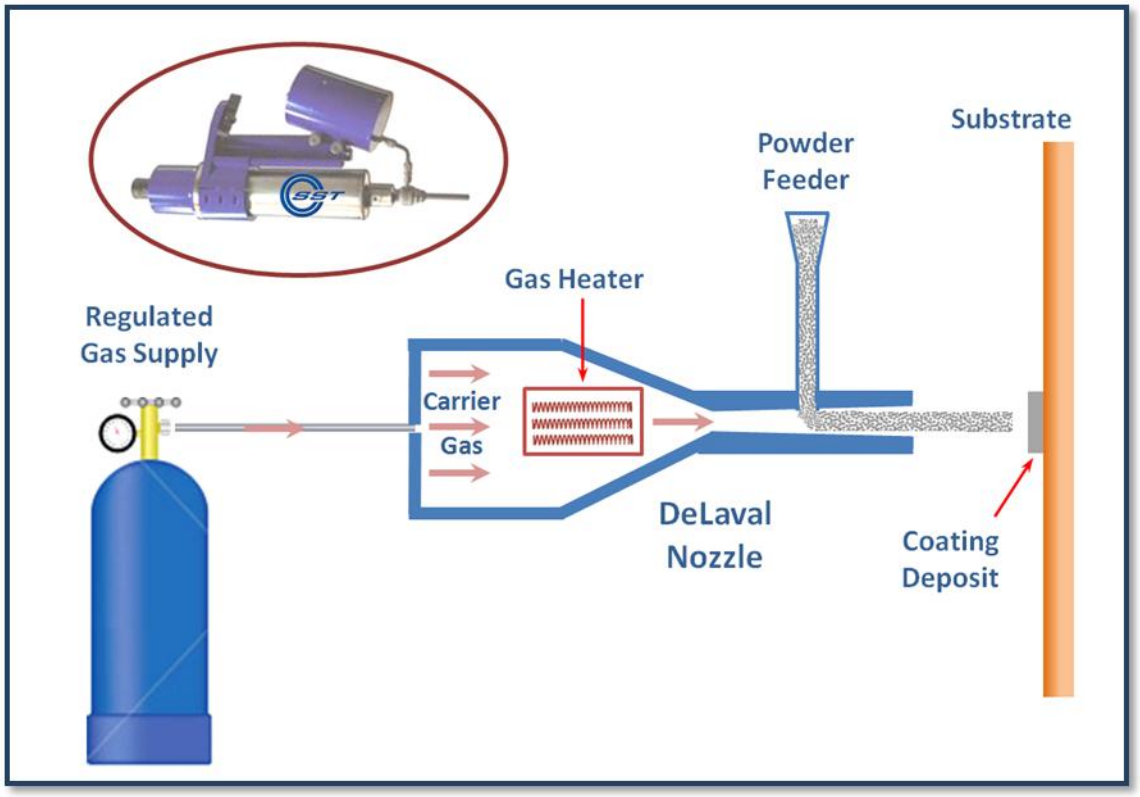

Figure 3.1. A Schematics of HPCS system (Courtesy of Centerline (Windsor) Limited).

The spraying gas was preheated to 365ºC to eliminate moisture in the feedstock powder. The recommended gas temperature is in the range of 0.2-0.3 of the melting temperature of feedstock powders **[1]**. The process parameters used by the high pressure cold spraying system to deposit all samples are listed in Table 3.2. It is worth mentioning that the process parameters used in this study were selected based on the lowest porosity within the coating microstructure among several combinations of spraying trials. It can be an interesting future study to precisely optimize the process parameters. The coating (Figure 3.2) was deposited at the thickness of 2 mm for all samples in this study.

Table 3.2. Operational cold spraying process parameters.

Process	Spraying parameters
Temperature (^oC)	350
Pressure (MPa)	1.75
Nozzle Stand-off (mm)	10
Gun Traveling Speed (mm/s)	25
Processing Gas	N_2

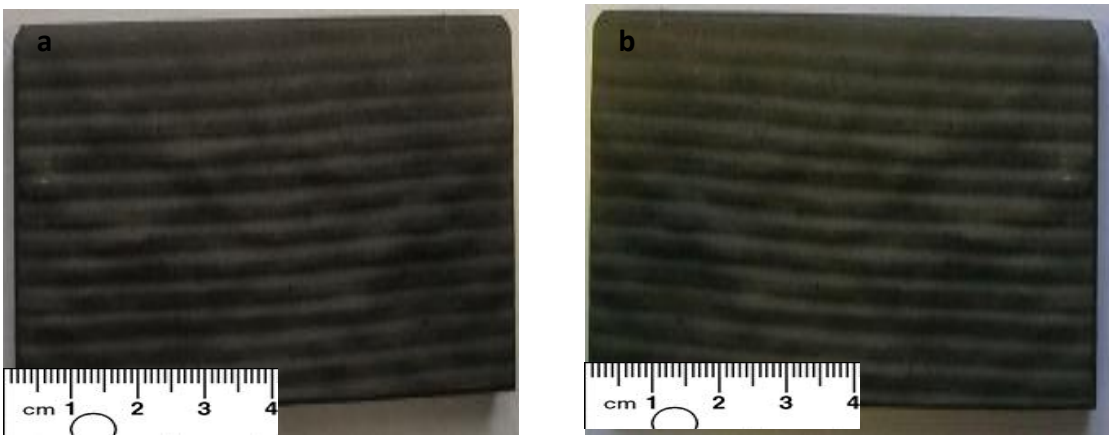

Figure 3.2. As sprayed Cold sprayed coatings (a) Blend I and (b) Blend II

3.3.2. Powder Metallurgy

The same composition as used for fabrication of cold sprayed samples (Pure Ni and 80 vol. % of Ni and 20 vol. % of Ni_3Al and pure Ni) was also used to fabricate samples using the P/M technique. A die was designed to manufacture a cylindrical P/M sample with 6.35mm diameter and 76.2mm length as shown in Figure 3.3. Cylindrical samples with 6.35 mm diameter and 76.2 mm length were fabricated using an in-house designed die. Following the conventional

P/M method, the samples were fabricated via several steps. The premixed powder was first poured into the die and cold pressed at 450 MPa, and then the die was placed inside a furnace at 500°C and pressed under 500 MPa pressure for further compaction.

Figure 3.3. Developed die used for P/M process in this study.

The samples were sintered at variable temperatures (500°C, 600°C, 700°C, and 800°C) for 2 hours at each temperature, followed by hot pressing. The optimal temperature and pressure for hot pressing of P/M samples were obtained through trial-and-error by varying the setup parameters, and the best results were obtained at 700°C. P/M processed samples that were processed via variable temperatures and pressures were then tested using optical microscopic and knoop indentation test. The optimal P/M samples were chosen based on having minimum porosity, highest density, and maximum hardness. Density measurements were performed on at least five P/M processed samples at each step consistent with ASTM-B311.The schematic of P/M process in this study is shown in Figure 3.4.

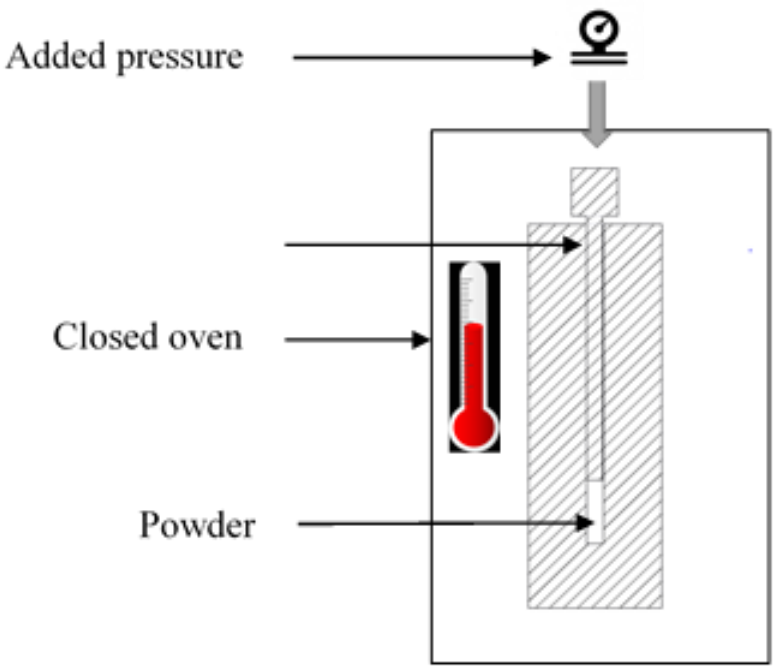

Figure 3.4. Schematic of P/M process used in this study.

3. 4. Microstructural Characterization

Cold sprayed and P/M processed samples were cross sectioned, ground, and polished before SEM and energy dispersive X-ray spectroscopy (EDS). SEM was performed on samples by a JEOL JSM-6490LV SEM (JEOL USA, Peabody MA, USA) using an accelerating voltage of 15 keV. A Nanotrace EDS detector equipped with a NORVAR light element window (ThermoScientific, Madison WI, USA) was used for elemental analysis by EDS. The morphology and the chemical analysis of the feed stock powders were also examined using above mentioned SEM equipment. Minimum of three EDS experiments at different regions of microstructure were performed on each sample.

Image analysis study was performed to determine the apparent porosity of the coatings and the P/M processed samples from the ten SEM images taken at various locations on each sample according to ASTM E 2109-00. According to the standard, image analysis must be

performed on micrographs at optimized magnification and size. The optimal magnification depends on the size and distribution of the microstructural features. A micrograph taken at very high magnification shows more details of microstructural features but does not represent a noticeable region in the microstructure. Reduction in magnification increases the area under investigation which results in less visibility of individual features in microstructure. After examining of several micrographs taken at different magnifications, those covering microstructural area of $520 \times 430\ \mu m^2$ were found to be the optimum for image analysis.

3. 5. Mechanical Characterization

A number of mechanical experiments were used in this study to evaluate the hardness and elastic modulus of the fabricated samples. Four different mechanical tests were used to better validate the hardness and elastic modulus results for the samples. All cold sprayed and P/M processed samples were cross sectioned, ground, and polished prior to harness testing.

3.5.1. Knoop Hardness Test

The Knoop indentation test is an appropriate method to measure hardness of coating structures due to the long rhombic shaped indenter that is capable to cover wide area containing splats, splat boundaries, and voids. In this study, Knoop hardness technique was conducted to simultaneously measure the Young's modulus of cold sprayed and P/M fabricated samples. An average of 12 Knoop hardness test were performed on each sample using a Zwick micro-hardness tester. It is possible to calculate Young's Modulus of materials using results from the Knoop indentation test according to Marshal's analytical equations. In this technique Young's modulus is measured based on the change in the length of the minor and major diagonals of the in-surface Knoop indentations $2b'$and$2a'$, respectively, after elastic recovery. Figure 3.5 shows a typical

Knoop indenter with diamond pyramid shape. A combination of elastic (reversible) and plastic (irreversible) regions will be resulted after Knoop indentation.

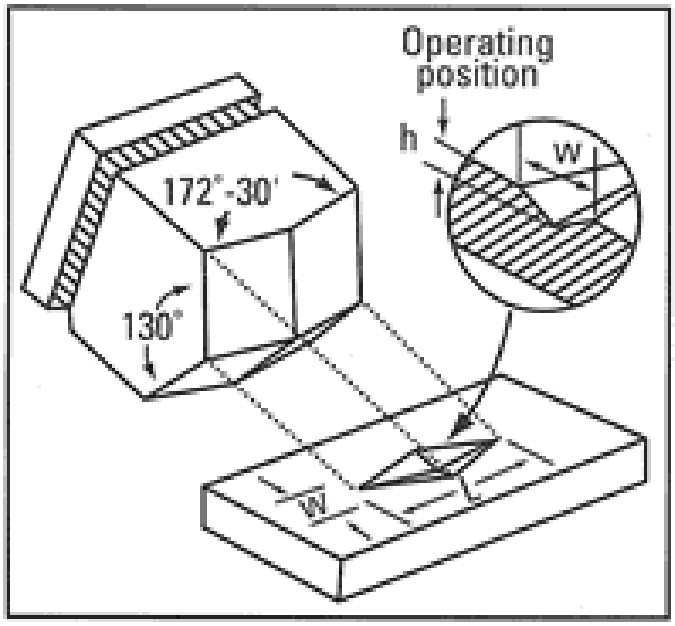

Figure 3.5. Schematic of the Knoop indenter geometry **[63]**.

The major and minor diagonals of the indentation start to recover after loading step which results in change in their length but this length change is negligible for the major diagonal as shown in Figure 3.6. The following equations relate the displacement of the minor diagonal 2b and H/E:

$$b - b' = \frac{\alpha a p}{E} \qquad \text{(Eq. 3.1)}$$

$$a - a' = \frac{\alpha b p}{E} \qquad \text{(Eq. 3.2)}$$

$$\frac{b\prime}{a\prime} = \frac{b\prime}{a} = \frac{b}{a} - \frac{\alpha H}{E} \qquad \text{(Eq. 3.3)}$$

Where H is Hardness, E is Young Modulus and $b'$and a' denotes the major and minor diagonal lengths of Knoop indentation afterward taking the indenter (after the elastic recovery). b and a are the major and minor diagonal of the indenter respectively. Where α is a constant value of 0.34 **[69]**.In the entirely loaded state, the ratio of the major and minor diagonals is $a'/\ b'$=7.11 which are defined by the indenter geometry **[73]**. Marshal et al. (1982) proposed this model to calculate the ratio of the Knoop hardness to elastic modulus **[73]**.

Average Knoop hardness was measured using fifteen indents on each sample with 1000gf load for 15 s. Knoop hardness can be calculated using the following equation;

$$HK = \frac{14.228P}{L^2} = \frac{P}{L^2 C_p} \qquad \text{(Eq. 3.4)}$$

Where L is the length of the major diagonal in mm, and P is denoted as the load in Kgf. C_p is a constant related to the length of the major diagonal.

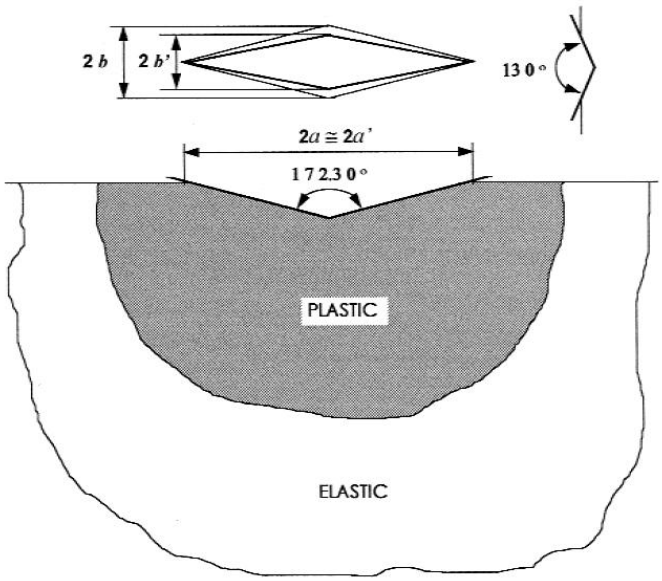

Figure 3.6. Elastic recovery of Knoop indentation after unloading **[63]**.

3.5.2. Vickers Hardness Test

Vickers test uses a square based pyramidal shape diamond indenter. The angle between the opposite sides of the pyramid is marked as 136° that is demonstrated in Figure 3.7. Vickers hardness is a function of the applied load (P) and the diagonal length (L) as shown in the Equation 3.5. Where angle θ equals to 136°.

$$H = \frac{2PSin\left(\frac{\theta}{2}\right)}{L^2} = \frac{1.854P}{L^2} \qquad \text{(Eq. 3.5)}$$

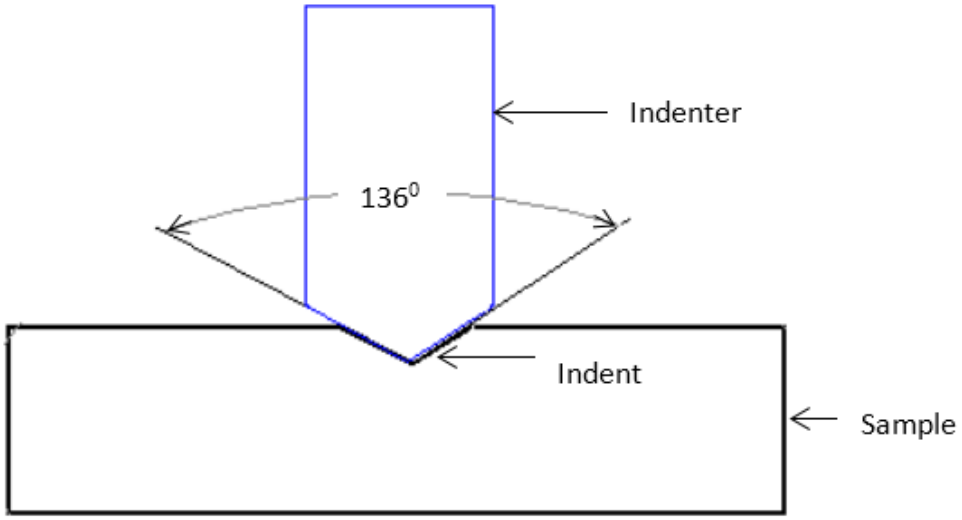

Figure 3.7. Schematics of Vickers indentation process.

Knoop hardness results were validated by conducting a Vickers hardness test using (Buhler Micromet 5140) on the same cold spray coating samples and P/M samples. Ten indents were used to obtain the average Vickers hardness with 1000gf for 15s. Unlike Knoop test, Vickers test can be very sensitive to applied load, where crack can propagate with plastic deformation by applying larger loads. Minimum of 15 Vickers indentation hardness tests were performed on the cross-section of each polished sample using a Buhler Micromet5140 micro-indentation hardness tester.

3.5.3. Nano-Indentation Test

Nanao-indentation is a mechanical characterization testing method that is also known as sub-micrometer indentation which is used to measure the elastic and plastic properties in very small scales. This technique was introduce over the last decade and currently it is widely been used to probe the mechanical properties of thin films due to higher accuracy and capability of

automation. There is several information we can obtain from the Nano-indentation test. Load versus displacement curve can be obtain from this experiment. The mechanical behavior of samples can be evaluated during the both loading and unloading steps. During the loading condition, with increasing the indentation depth; elastic and plastic deformation will occur. Then at the unloading step, where the load is slowly released; the material will deform elastically. The hardness can be calculated by application of mean pressure during indentation at maximum load. Scratch testing, hardness and elastic modulus can be obtained in ceramic, metals, glasses and polymers using nano-indentation test.

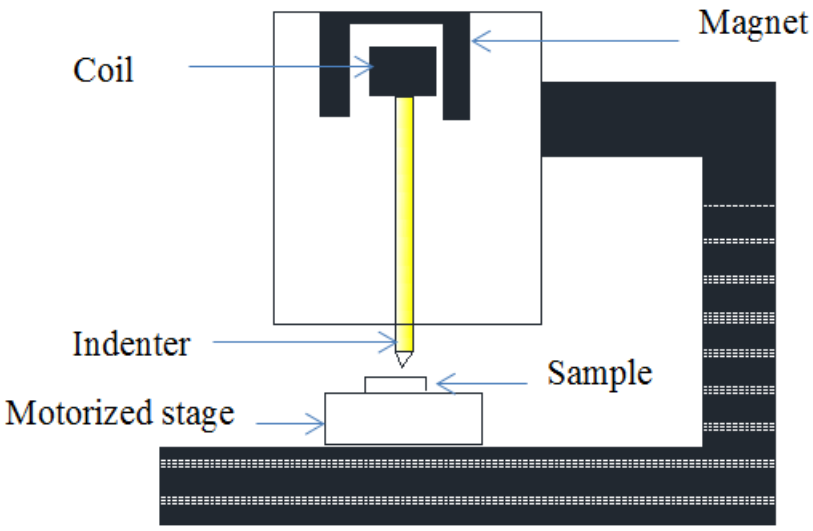

Figure 3.8. Schematics of Nano- indentation test.

In the present study Nano-indentation test was used to measure the elastic modulus of fabricated samples. A Tribo-indenter 900 (Hysteron Inc.) was used with a Berkovich indenter under quasi-static mode to determine the reduce modulus. Schematic of nano- indentation is illustrated in the Figure 3.8. Thirty indentations were made for each sample to obtain an average value of the samples' elastic modulus. Zeng and Fisher (2009) proposed a method to calculate a

reduce modulus from the values obtained from the direct measurements from the nano-indentation test **[67]**. Equation 3.6 shows the relationship between the reduced modulus , E^* with v_s the Poisson's ratio of the flat surface, E_s - modulus of elasticity of the flat surface of the sample, v_i- Poisson's ratio of the sphere, and E_i- modulus of elasticity of the sphere **[64][65].**

$$\frac{1}{E^*} = \frac{(1+{v_s}^2)}{E_s} + \frac{(1+{v_i}^2)}{E_i} \qquad \text{(Eq. 3.6)}$$

3.5.4. Resonance Frequency Test

This technique was established in 1938 to obtain resonance frequency of concrete by matching the tone created by musical instrumentation **[66]**. Overtime this technology was developed by introducing more controls and electronics. The Resonant Frequency Analyzer (RFA) is also used to measure long term deterioration properties of concrete blocks **[67]**. The test is is also capable of measuring dynamic modulus of elasticity of subsided metal samples. Rayleigh derived Equation 3.7 to calculate the dynamic modulus of elasticity (E) using flexural vibration of a thin rod **[67]**.

$$E = \frac{4\pi^2 L^4 N^2 d}{m^4 K^2} \qquad \text{(Eq. 3.7)}$$

where, d , $L, N, k,$ and t are density of the material, length of the specimen, fundamental flexural frequency, radius of gyration of the section about an axis perpendicular to the plane of bending, and thickness of the sample, respectively. m is constant equal to 4.73.. Equation 3.7 can be used in two different modes, where the rod is vibrating in flexure free mode or in the longitudinal mode [**64**]. The schematic of typical RFA apparatus is illustrated in Figure 3.9.

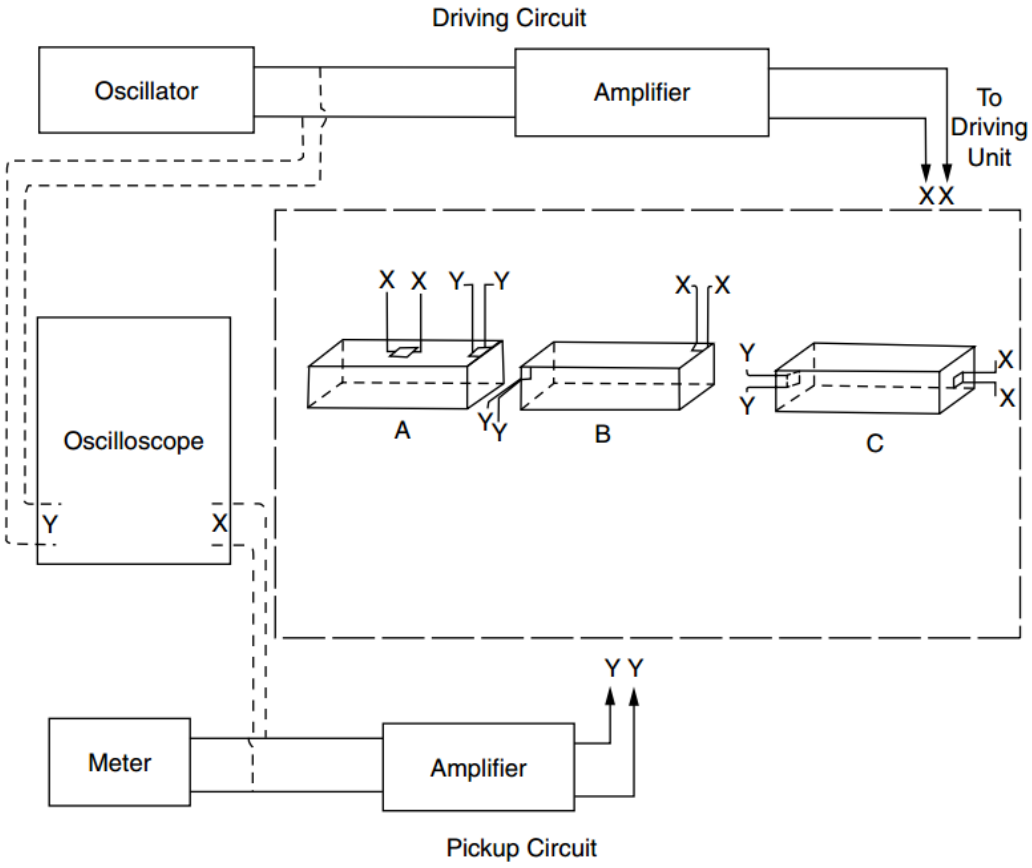

Figure 3.9. Schematic of RFA including three types of vibrations modes (A) Transverse resonance (B) Torsional resonance (C) Longitudinal resonance **[68]**

In the current study, the validation of the measurements of elastic moduli was performed using a RFA by IMCE, Belgium. The cold sprayed samples and P/M samples were prepared according to ASTM E 1876 for the RFA tests. Due to the size limitation of fabricated samples, the cold sprayed samples were cut to rectangular strips of 50 mm L × 10 mm W× 2 mm T, and the P/M samples were cut into cylindrical shapes in the size of 6.35 mm D × 50 mm L. The average elastic modulus value was obtained from three different RFA tests on each sample. The obtained elastic moduli from RFA tests were compared to the ones resulted from nano-indentation and Knoop hardness test.

CHAPTER 4. RESULTS AND DISCUSSION

4.1. Overview

This chapter presents the results of the experiments that were described in Chapter 3. Sections 4.2 presents the results of the experiments performed to characterize the microstructure of the feedstock powder, cold sprayed and P/M processed Ni and Ni-Ni_3Al samples. Section 4.3 presents the results of the mechanical tests (Vickers, Knoop, Nano-indentation, and Resonance Frequency) performed on all samples in this study.

4. 2. Microstructural Characterization

Figure 4.1 (a) and (b) show the SEM micrographs of pure Ni powder and Ni_3Al powder used in this study, repectively1q. The SEM micrograph of the 80 vol. % of Ni and 20 vol. % of Ni_3Al powder mixture is shown in Figure 4.1 (c). Ni powders as seen in Figure 4.1 (a) and (c) were agglomerated and formed tangled particles, causing a branched type geometry, which does not reflect the nominal particle size reported by the manufacturer. However, the measured average size for Ni_3Al particles was 24.53±15.57 μm. The large scattering indicated the large variety in the particle sizes of Ni_3Al powders. Table 3 lists the chemical composition of each region obtained by EDX experiment. The average weight percentage of each phase was determined based on 3 different measurements.

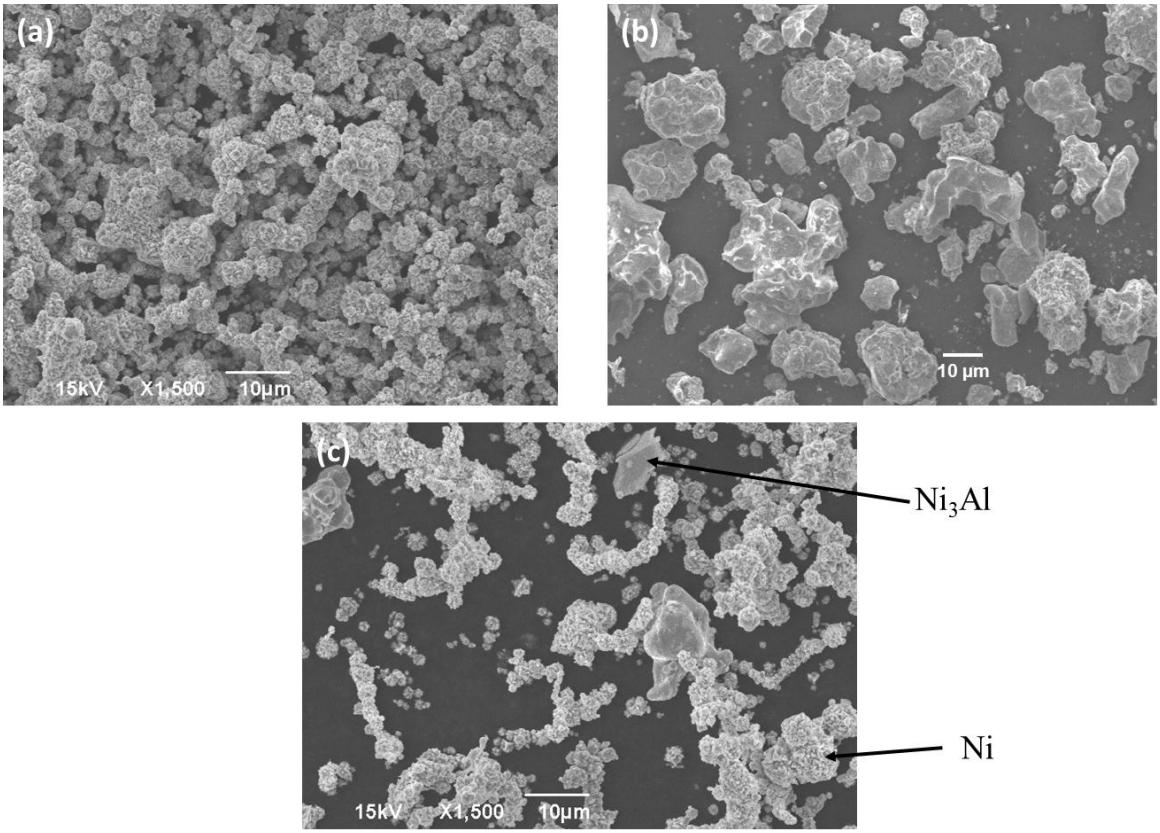

Figure 4.1. SEM images from feedstock powders of (a) Ni, (b) Ni_3Al, and (c) mixture containing 80 vol. % Ni and 20 vol. % Ni_3Al.

The EDX results confirmed that the commercially obtained Ni powder had purity more than 99.6% and Ni_3Al had 85.7 wt. % of Ni and 14.2 wt. % of Al. The Ni-Al phase diagram reports85-87 wt. % of Ni and 13-15 wt. % of Al in Ni_3Al, which is in very good agreement with the EDX results obtained in this study **[1]**.

Table 4.1. Chemical compositions of feedstock powder shown in Figure 4(c).

Phases	Nickel (wt. %)	Aluminum (wt. %)
Ni_3Al phase	85.7 ± 2.8	14.2 ± 1.3
Ni phase	99.63 ± 1.8	0.37 ± 0.06

Figure 4.2(a) shows SEM micrograph of the cross-sections of cold sprayed Ni sample. The areas of two distinct contrasts were visible in this micrograph. The gray (region 1) and black (region 2) regions represent Ni and porosities respectively in the cold sprayed Ni coatings. This was validated by EDX results listed in Table 4.2. The micrograph shown in Figure 4.2(b) shows cross-section of cold sprayed Ni-Ni_3Al sample. Regions of three different contrasts are clearly illustrated in this image: light gray, dark gray, and black. EDX experiment identified those regions as Ni, Ni_3Al and porosity, respectively. It has been tried to find an optimized resolution and magnification for micrograph images used for image analysis. The micrographs taken at the magnification shown in Figure 4.2(a) and (b) could better show distribution of particles in a region representing a distinct portion of microstructure. Six different SEM images taken from each sample were subjected to the image analysis to identify the area percentages of different phases within the coating microstructure, and the results are listed in Table 4.3. The inset image shows higher magnification micrograph of selected area as marked in Figure 4.2 (b). This image taken at higher magnification provided us with more information regarding the bonding between Ni_3Al particles and Ni matrix. Although, there is good cohesion between particles and matrix, a separation line can be seen at some interface regions. Some porosity can also be seen along the interface.

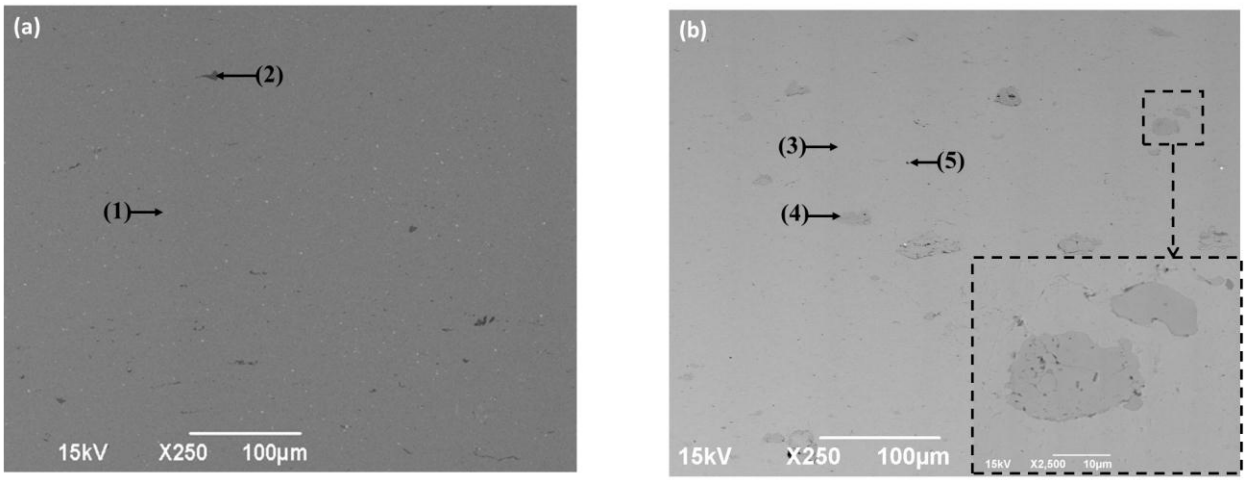

Figure 4.2. SEM micrographs of cold sprayed (a) Ni, and (b) Ni-Ni_3Al coatings. The inset of Figure 4.2(b) shows higher magnification image of selected area.

Table 4.2. Chemical compositions of cold sprayed coatings obtained from EDX as marked in Figure 4.2.

Location	Nickel (wt. %)	Aluminum (wt. %)
Region 1	99.9±0.01	---
Region 2	---	---
Region 3	99.91±1.1	0.09±0.01
Region 4	78.77±1.7	21.23±2.1
Region 5	---	---

The image analysis results showed that the microstructure of MMC contained around 92 area % of Ni and 8 area % of Ni_3Al. Considering the 20 vol. % of reinforcement added to the matrix, the image analysis results showed reduction in reinforcements after the cold spraying deposition. Some Ni_3Al particles, being the harder phase, could be crushed and disappeared during the spraying process. However, the main reason associated with this discrepancy could be that the softer Ni particles underwent more deformation during the spraying impact while the

harder Ni_3Al particles subjected to less deformation and kept their original aspect ratios. The 2D SEM images were unable to capture the third dimension of the Ni_3Al particles and use it in image analysis.

Table 4.3. Area percentage of different phases in cold sprayed coatings.

Sample	Ni Area%	Ni_3Al Area %	Voids Area %	Impurity Area %
Ni- Ni_3Al	91.738 ± 1.43	7.973 ± 1.24	0.205 ± 0.04	N/A
Ni	95.34 ± 2.88	---	0.41 ± 0.25	4.25 ± 1.12

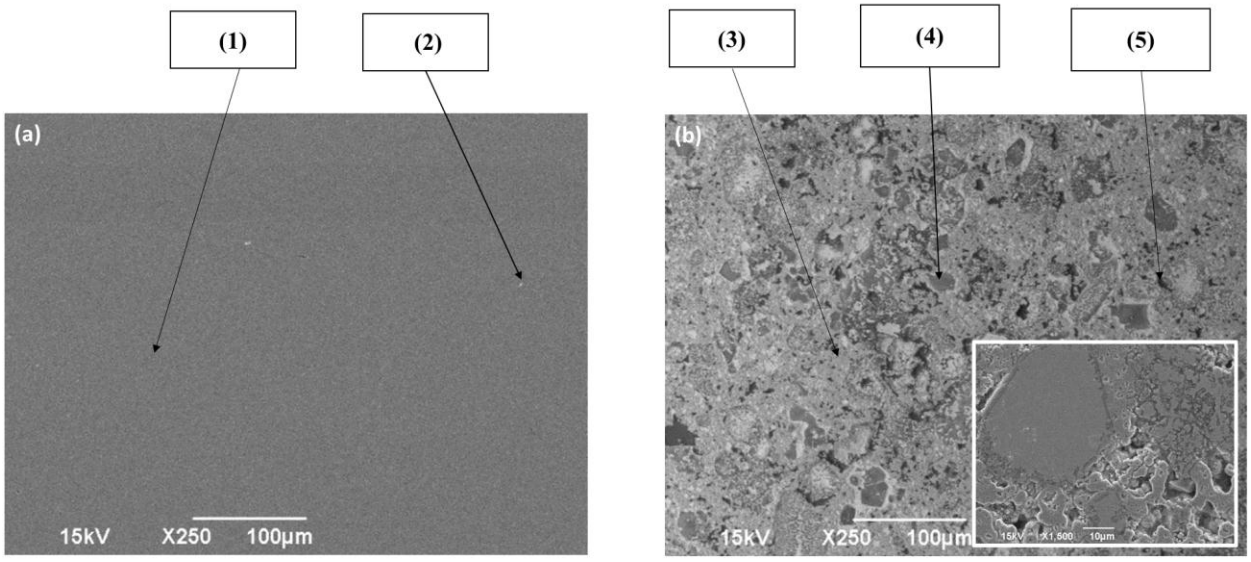

Figure 4.3. SEM micrographs of P/M processed (a) Ni, and (b) Ni-Ni_3Al coatings. The inset of Figure 4.3(b) shows higher magnification image of microstructure.

Figure 4.3 shows the SEM images of the P/M processed Ni and Ni-Ni_3Al samples fabricated in this study. The microstructure of unreinforced Ni sample shown in Figure 4.3(a)

represents a bulk and dense structure, while the SEM micrograph of Ni-Ni_3Al shown in Figure 4.3(b) contains three different contrast levels that could also be observed in cold sprayed samples. The micrograph of randomly selected area inset of Figure 4.3(b) shows the microstructural features in higher magnification. EDX results indicated that the chemical compositions in the light gray and dark gray regions are Ni and Ni_3Al, respectively, while the black areas represent voids as listed in Table 4.4.

Table 4.4. Chemical compositions of P/M samples obtained from EDX as marked in Figure 4.3.

Phase	Nickel (wt. %)	Aluminum (wt. %)
Region 1	99.9 ± 0.01	---
Region 2	---	---
Region 3	99.82±0.95	---
Region 4	86.22 ± 0.22	13.78 ± 0.85
Region 5	---	---

* Average of 3 measurements ± 1 standard deviation

Table 4.5 presents the results of image analysis conducted on six different SEM images with similar magnification as Figure 4.3(a) and (b) taken from various regions of pure Ni samples and reinforced P/M samples. The area percentage of the Ni_3Al reinforcement phase is higher in P/M samples compared to the cold sprayed ones. This could be mainly attributed to the shattering or possibility of the hard Ni_3Al particles bouncing off during the impact on the substrate which resulted in a reduction of reinforcement in the cold sprayed samples. However,

the measured porosity levels in all the P/M samples (reinforced and unreinforced) were much higher than the same ones produced by cold spraying.

Table 4.5. Area percentages of different phases in P/M samples.

Sample	Ni	Ni_3Al	Voids
Ni-Ni_3Al P/M	78.1 ± 3.29	19.1 ± 1.21	2.8 ± 1.18
Ni P/M	99.92 ± 0.11	---	0.08

* Average of 6 measurements ± 1 standard deviation

The amount of porosity and their geometry and shape are considered as critical parameters that define properties of the material. The majority of porosities in the P/M samples had relatively larger sizes with irregular shapes where they were finer and round in the cold sprayed samples. The pure Ni samples manufactured by P/M showed less visible porosities compared to the reinforced P/M samples, and that might be due to the same particle size in both P/M and cold spraying processes of Ni samples. Although, the differences in particle sizes between Ni and Ni_3Al particles exist in powders used in both fabrication techniques, the P/M processed samples may have been affected more due to the particle size mismatch of the two types of powers during the pressing steps of the P/M fabrication process. It is believed that the effect of particle size mismatch is less for the cold spraying process because sprayed particles impact and flatten on the previously deposited particles, and therefore the sprayed particles will have less effect on the porosity formation compared to those partially deformed particles during the P/M process.

SEM micrographs obtain from pre mixed blend (I) and blend (II) are shown in Figure 4.4 (a) and (b) respectively. From the given information and the similar contras levels from the

images below, it is difficult to differentiate the Ni and Ni_3Al particles separately. Even though the mixing ratios between the Ni and Ni_3Al are 80% to 20%, SEM images do not provide distribution clearly due to similar contras. However by further examination Ni and Ni_3Al particles are identified with variable shapes and marked in the images. Using the EDX results, it was confirmed that blend (I) and (II) carry Ni and Ni_3Al to proper ratios. The results acquired are listed in Table 4.6.

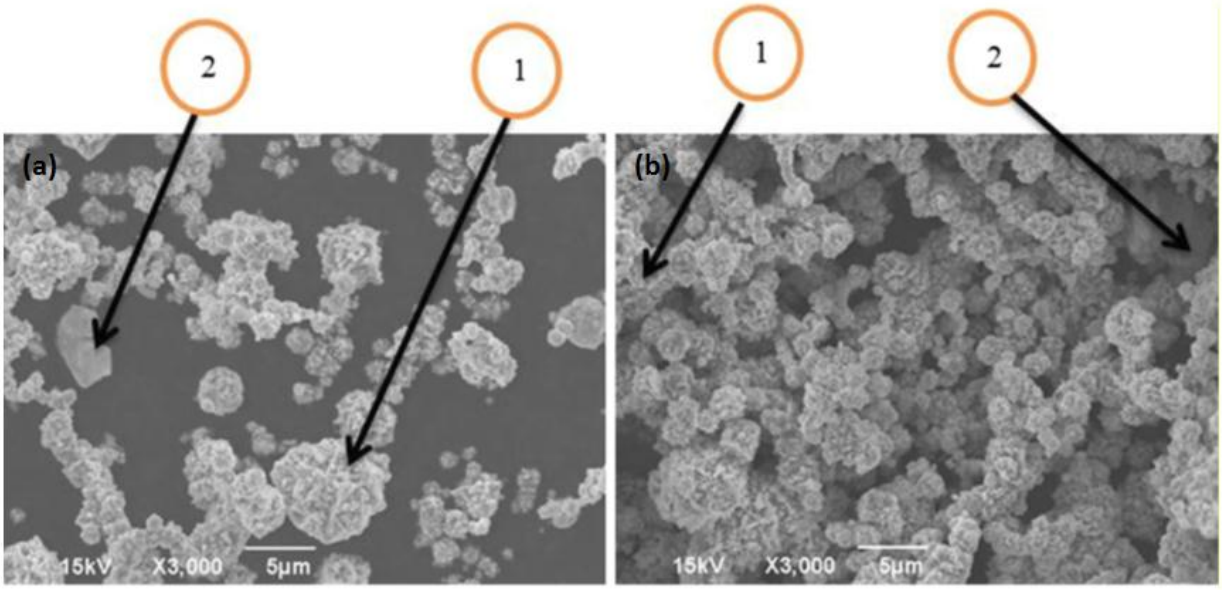

Figure 4.4. SEM micrograph of cold spraying feedstock powder of (a) Blend (I), and (b) Blend (II).

Table 4.6. Chemical composition by weight percentage in coatings according to Figure 4.4(a) and (b).

	Nickel (wt. %)	Aluminum (wt. %)
Blend (I)—(1)	85.7±2.8	14.2±1.3
Blend (I)—(2)	99.63±1.8	0.37±0.06
Blend (II)—(1)	79.33±4.1	19.3±2.8
Blend (II)—(2)	99.67±0.9	0.33±0.08

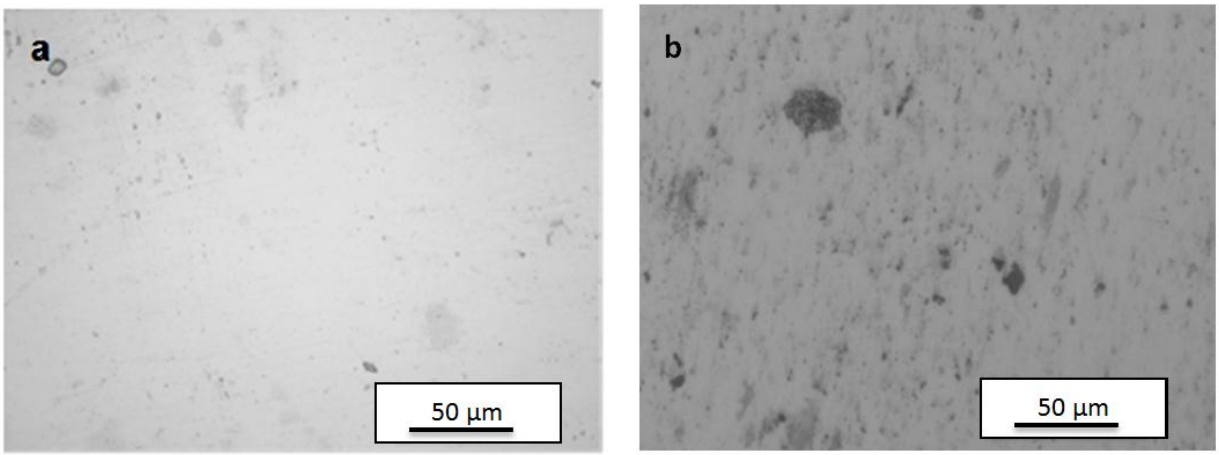

Figure 4.5. Optical image of cold sprayed coatings of (a) Blend (I), and (b) Blend (II).

Apart from the SEM images, the optical micrographs were taken from the fabricated samples to observe the particle distribution, porosity and spat boundaries in the microstructure as shown in Figure 4.5(a) and (b) . However the optical images were unable to provide any good information, hence the higher magnification SEM images were used to observe microstructure of the samples, where Figure 4.6(a) and (b) illustrate the cold sprayed samples fabricated from blend (I) and (II) respectively. Using the EDX, the three different contras levels of gray, dark

gray and black and shown in the images were distinguished as Ni, Ni_3Al and voids. This microstructural observation was validated using EDX results that are listed in Table 4.7. Figure 4.6 (b) illustrates that the average particle size of Ni_3Al is much lower than the actual size of feedstock particle size of >45 μm to <100 μm. The high velocity deposition of particle can cause particles to deformed and shattered to smaller in size particles.

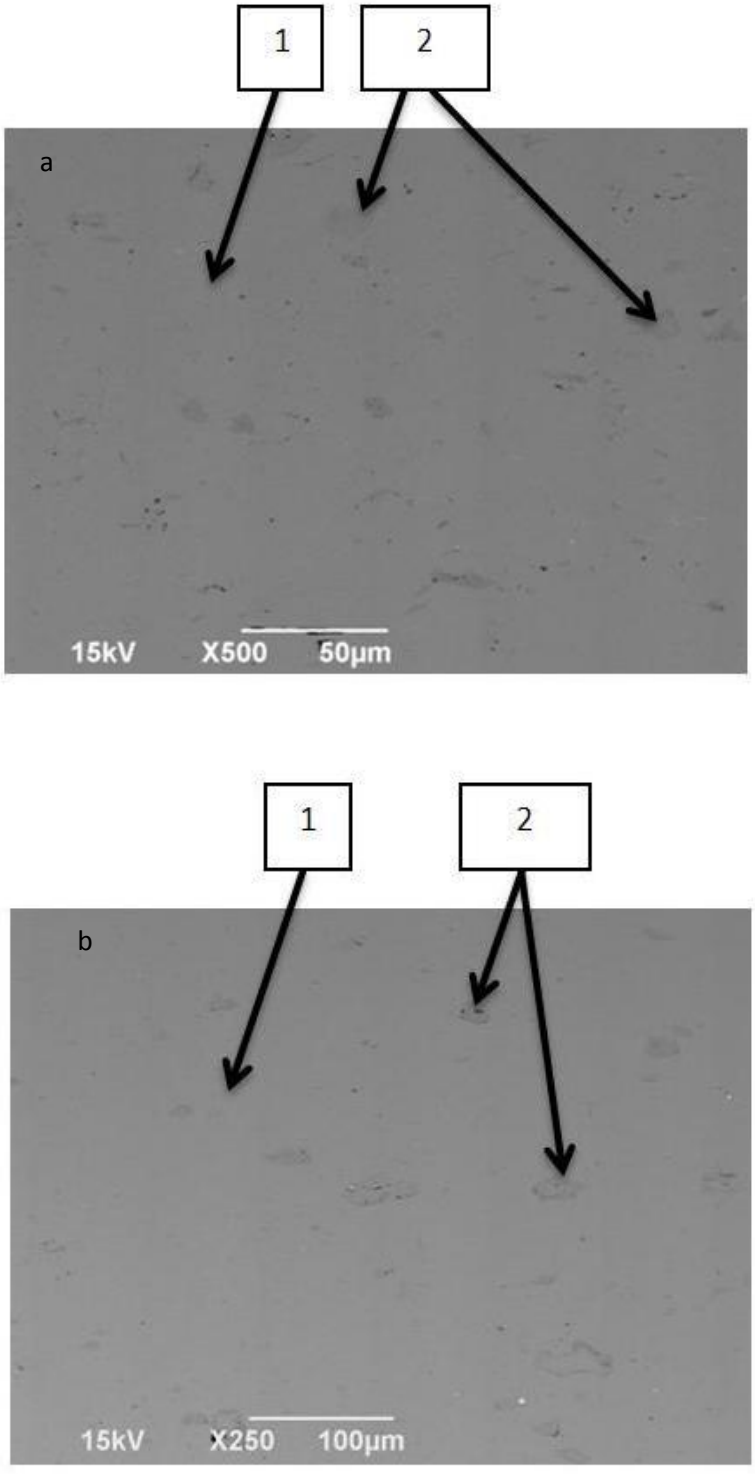

Figure 4.6. SEM micrograph of cold sprayed coatings of (a) Blend (I), and (b) Blend (II).

Three different SEM images from each cold spray samples were used to obtain the average porosity, and the area percentage of the Ni and Ni_3Al. The average values obtained using image analysis method is listed in Table 4.8. Image analysis results shows that the area percentage of Ni_3Al in both blend (I) and (II) are less than 8% of the total area. However the fabricated samples contained 20% vol. of Ni_3Al. The lower area percentage of reinforcement particles could be due to the shattering and bouncing back from the coating surface. Apart from that, the comparison of volume (3D) vs area (2D) could affect the amount of particle distributed.

Image analysis indicates that smaller particle reinforcement (blend I) has slightly created more porosity compared to larger particles (blend II). However there is no significant difference in area percentages of matrix and reinforcement among the two samples, the porosity presents in the sample. Overall reinforced samples fabricated with cold spraying with two different blends have porosity level below 0.25%.

Compared to the other thermal spraying techniques available, cold spray is capable of eliminating solidification and melting in the microstructure that could results is lower amount of porosity **[69]**. Bashirzadeh et al. (2014) observed this phenomenon in cold prayed Al-Cu composites, however this cannot considered as a universal statement which has an effect on cold sprayed coatings in general **[69]**. Compared to Ni samples fabricated from cold spraying, MMC samples contained much lower porosity levels. Few studies were done to see the effect of particle size on the velocity variation, and, it was shown that smaller particles carry higher velocity which leads to belter mechanical interlock that create strong bonding among adjacent particles**[59][60][70][71][74]**. The bonding mechanism term “Interlock” is commonly used in thermal spraying process to describe the mechanical bonding in coatings. This causes to form less porosity in blend (I) MMC coatings compared to larger blend (II) coatings. Hence this

study clearly shows that MMC fabricated from cold spraying with smaller Ni_3Al reinforced particles has better bonding with low porosity.

Table 4.7. Chemical composition by weight percentage in coatings according to Figure 4.6.

	Nickel (wt. %)	Aluminum (wt. %)
Blend I –(1)	99.82 ±1.5	0.18% ±0.02
Blend I- (2)	78.77 ±1.7	21.23% ±2.1
Blend II- (1)	99.81 ±1.6	0.19% ±0.04
Blend II- (2)	77.3.3 ±3.1	22.67% ± 2.7

Table 4.8. Area percentage of existing phases in the cold sprayed samples.

Sample area %	Ni	Ni_3Al	Voids
Blend I	91.738 ±1.43	7.973±1.24	0.205±0.04
Blend II	92.969±0.94	7.069±0.87	0.197±0.07

4. 3. Mechanical Characterization

The results of Vickers and Knoop hardness tests on the reinforced and unreinforced cold sprayed and P/M processed samples are listed in Table 4.9. The Ni-Ni_3Al composites exhibited higher hardness values compared to the pure Ni samples regardless of manufacturing method. The obtained hardness value of P/M processed Ni sample is close to the lowest hardness value reported for the bulk Ni which ranges from 400 to 600 HV **[1]**.

Table 4.9. Hardness results of cold sprayed and P/M samples.

	Vickers hardness (HV)	Knoop hardness (HK)
Ni-Ni_3Al cold sprayed	427.5± 8.2	398.4± 17
Ni cold sprayed	413.2 ± 6.9	377.9 ± 9.05
Ni-Ni_3Al P/M	391.7 ± 4.6	373.1 ± 10.4
Ni P/M	384.4 ± 7.5	359.9 ± 4.7

The elastic moduli of the cold sprayed and P/M processed samples were calculated from Marshal's equation using Knoop hardness values. The calculated elastic modulus were obtained using 3 equations based on the Marshals method mentioned in section 3.5.1 which resulted in Equation 4.1 and the results are listed in Table 4.10.

$$\left(\frac{b'}{b}\right) = 1 - 2[(1 - v^2)\tan(\gamma)]\left(\frac{HK}{E}\right) \qquad \text{(Eq. 4.1)}$$

Where v represents Poisson's ratio and γ is the standard half-angle of Knoop indenter equal to 75º. HK is the Knoop hardness. b' denote the diagonal length of Knoop indentation afterward taking the indenter. b is the major diagonal of the indenter.

Table 4.10. Calculated and experimentally obtained elastic modulus of cold sprayed and P/M samples.

Fabrication Process	Materials	Marshall Equation (GPa)	Nano-indentation (GPa)	Resonance frequency (GPa)
Cold Spray	Ni-Ni_3Al	152.18± 10.1	191.6 ± 10.49	193.2 ± 0.4
	Ni	143.8 ± 8.7	199.3± 13.1	182.4 ± 0.1
P/M	Ni-Ni_3Al	146.1 ± 5.0	161.5 ± 12.9	70 ± 0.01
	Ni	131.0± 6.2	148.2 ± 6.22	66.39 ± 0.01

Marshall has rearranged the Equation 4.2 and presented in a simpler manner to obtain the elastic modulus using Knoop hardness (*HK)* , major and minor diagonal of indentation after elastic recovery (*2a'* and *2b'* respectively) and initial major and minor diagonal of indenter (*2a* and *2b* respectively*)*.

$$E = \frac{\alpha_1 HK}{\left(\frac{b}{a} - \frac{b'}{a'}\right)} \qquad \text{(Eq. 4.2)}$$

Where, α_1 is a constant value of 0.34 **[73]**, v represents Poisson's ratio and γ is the standard half-angle of Knoop indenter equal to 75º.

Nano-indentation and resonance frequency tests were also used to experimentally measure the elastic modulus of all samples in this study. Comparison between the obtained results from variety of testing methods will show the capabilities of each of those techniques in accurately measuring the properties of cold sprayed and P/M processed samples. The elastic modulus obtained from Knoop test and marshal equation had the lowest value for all samples compared to the other two techniques. The elastic modulus values obtained from both nano-

indentation and resonant frequency tests on cold sprayed Ni samples were in an acceptable range between the value reported for cold sprayed Ni coating, 158±6GPa, and bulk Ni material, 207±11 GPa **[8][74]**. There is an increasing trend in elastic modulus of cold sprayed Ni samples with addition of Ni_3Al particles. Since the porosity is negligible in both cold sprayed Ni and Ni-Ni_3Al samples according to Table 4.8, the main reason for increase in elastic modulus of Ni-Ni_3Al samples can be attributed to the higher strength of hard Ni_3Al particles and strong bonding and interface between matrix and particles as it can also be seen in inset of Figure 4.2 (b). However, results obtained from nano-indentation test showed no significant improvement in the elastic moduli of cold sprayed Ni samples after addition of Ni-Ni_3Al particles. It could be due to the fact that small Berkovich indenter was unable to measure the hardness in the area which represents all features within the microstructure.

The calculated and experimentally measured elastic moduli of the P/M samples are listed in Table 4.10. The reinforced P/M samples had higher elastic modulus values compared to the unreinforced ones. Similar to the hardness, the elastic modulus of the fabricated P/M Ni samples is also much lower than that of the industrially fabricated bulk Ni at room temperature which is around 200-210 GPa **[8]**. However, the reinforced P/M samples have slightly higher elastic modulus values compared to pure Ni samples due to the anomalous behavior of Ni_3Al which increases the precipitation hardening and dislocation, leading to increased elastic modulus **[25][26][27]**. The elastic modulus obtain from P/M samples (Table 4.10) using resonance frequency test illustrates lower values compared to the other mechanical testing. Though RFA is a great technique to obtain elastic modulus using the vibration; having voids in P/M samples could add errors to the results. The voids can act as a vibration damper or absorber that result in lower values of modulus.

None of the above mentioned manufacturing techniques includes melting and solidification of the particles during the fabrication process. The bonding of the sprayed particles is purely due to the interlock between impacted and deformed solid powders. There is no metallurgical bonding between the particles in cold sprayed samples and mechanical bonding is the only reason for adhesion between the splats and the coating layers. The solid particles were partially deformed during mechanical pressing and attached to each other in P/M process. It is known that the sintering process may cause some diffusion between elements resulting in local metallurgical bonding in P/M processed samples. The results from this study showed that the mechanical interlock in cold sprayed samples is stronger than the metallurgical bonding in P/M processed samples.

The results obtained in this study proved the strengthening of Ni material with the addition of Ni_3Al particles. Comparison between the elastic moduli obtained using Marshal's equation and resonance frequency for unreinforced and reinforced Ni materials are shown in Figure 4.7. The results from Marshal's equation indicated that the addition of Ni_3Al particles was more effective in improving elastic modulus of Ni in P/M processed samples. The addition of harder phase, Ni_3Al, resulted in the increase of the average hardness of the P/M processed samples, and consequently, the elastic modulus of the P/M processed material was also increased according to the Marshal Equation. Alternatively, the elastic modulus obtained from the resonance frequency technique depends on the bonding mechanisms, porosity content, and interfacial properties between the particles and the matrix. According to the results obtained from the resonant frequency test, P/M processed samples exhibited significantly lower elastic moduli compared to cold sprayed ones due to their relatively higher porosity and lower bonding strength between partially compacted particles. The addition of 20 vol. % Ni_3Al particles had a slight

effect on improvement of the mechanical strength in the pure Ni P/M processed samples according to the resonant frequency test. Further investigation at different percentages of the reinforcement phase can help to better understand the effectiveness of Ni_3Al on mechanical properties of P/M processed samples.

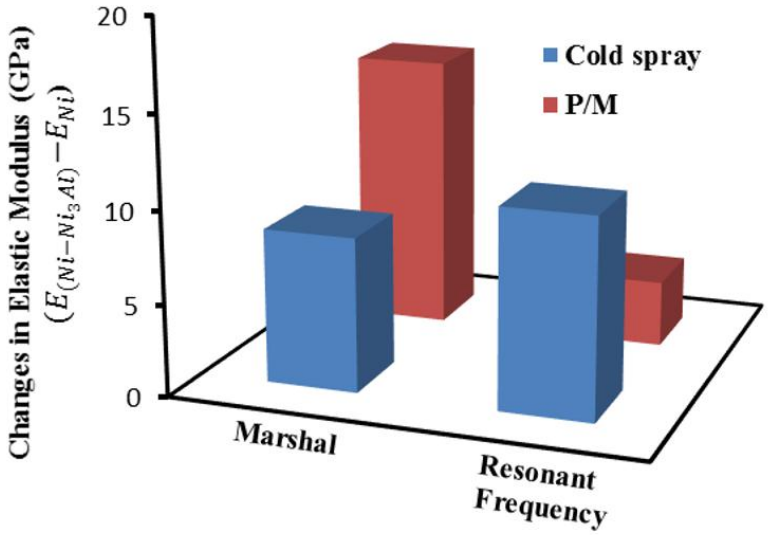

Figure 4.7. The increase in elastic modulus of Ni samples after addition of Ni_3Al obtained from Marshal and resonant frequency test.

Shallow and long rhombic shaped indents have made Knoop indentation well known for testing hard-brittle materials. SEM micrograph of a Knoop indent on a cold sprayed sample is shown in Figure 4.8. For this sample, the average Knoop hardness value of blend (I) was 398.4±17 HK and blend (II) was 370.2±5.2 HK. Similarly, the calculated average elastic modulus for blend (I) was 152.18±10.1 GPa and blend (II) was 138.5±10.1 GPa. Some cracks are visible in the Ni matrix as a result of the Knoop test in Figure 4.8. However, the crack propagation was hindered by Ni_3Al particles which have the ability to block crack growth within composite microstructures. Therefore a larger number of Ni_3Al particles should be distributed in

the matrix of composite fabricated using blend (I) as it showed more obstacles for crack propagation as opposed to blend (II). The above assumption can be made due to the fact that both composites consisted of 20% vol. of the reinforcement phase.

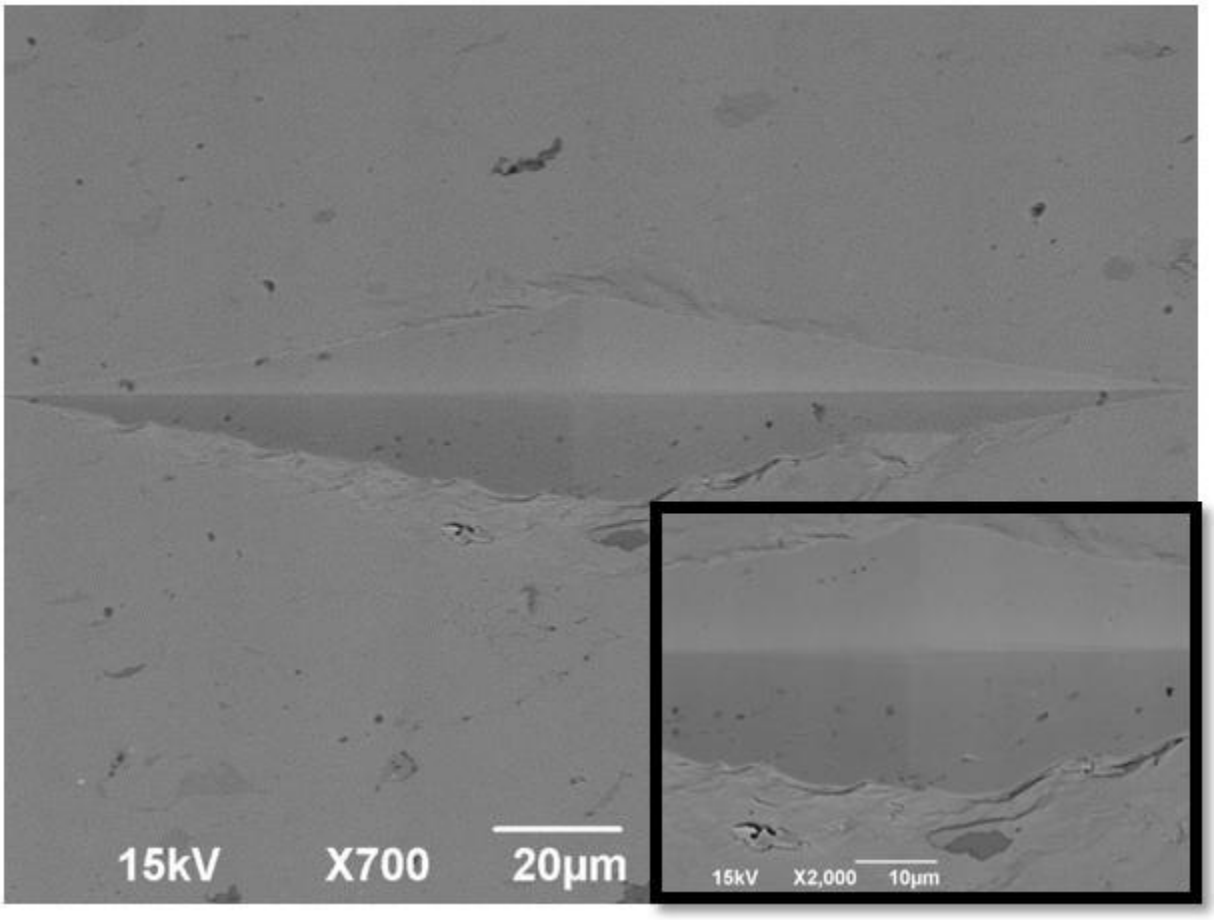

Figure 4.8. SEM micrograph of a Knoop indentation, the inset is the portion of similar indent at higher magnification.

Vickers hardness test was used to validate results from the Knoop indentation test and also to measure the hardness properties of the cold sprayed samples. The Vickers hardness value for blend (I) was 427.5±8.2 HV and blend (II) was 422.5±14.36 HV. This result was similar in trend to those results from the Knoop indentation tests. Figure 4.9 shows an optical microscope

micrograph of a Vickers indentation made on a cold spray sample. Similar to Knoop indentation, Vickers indentation also results in some cracks on the Ni matrix.

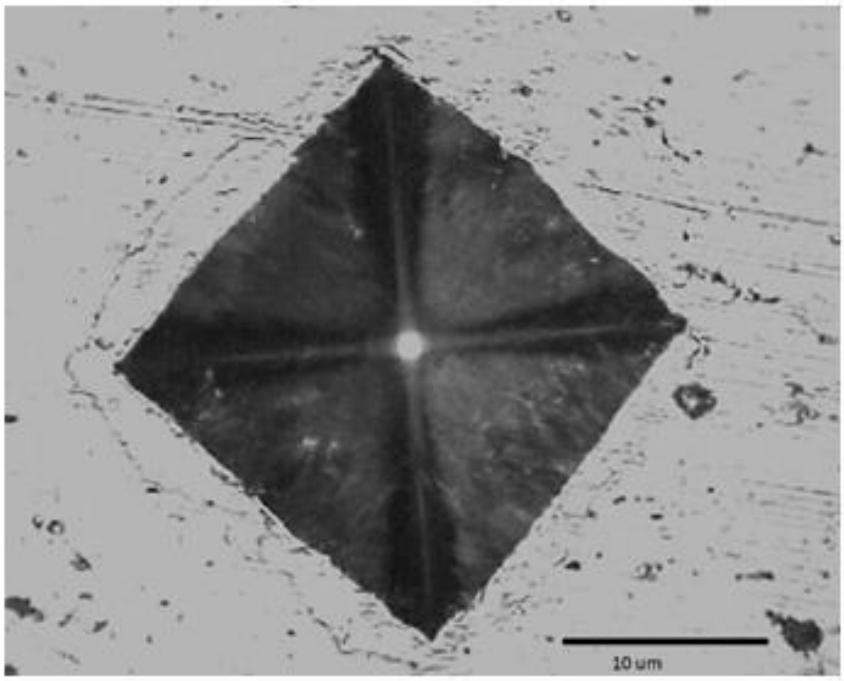

Figure 4.9. Optical micrograph of a Vickers indentation on Ni-Ni_3Al < 45 μm (Blend I).

The hardness of individual splats and phases within microstructures of coating materials can be measured using nano-indentation tests. Nano-indentation tests can also be used to determine the modulus of elasticity. Load vs. displacement curves from 10 different nano-indentation tests on blend (I) can be seen in Figure 4.10. An image of the corresponding series of indents made by the nano-indentation is shown as inset to Figure 4.10. For this test the maximum load of the cold sprayed samples was kept at 9000 μN in order to avoid any plastic deformation.

The calculated curve of average values for the load vs. displacement results from the 10 nano-indentation tests on blend (I), blend (II) and on pure nickel can be seen in Figure 4.11. Cold sprayed pure nickel was used here as a reference for blend (I) and (II). Figure 4.11 illustrate that

blend (I) and blend (II) has higher elastic modulus and hardness compared to pure nickel and in addition it indicates that blend (I) has less displacement as opposed to blend (II). Blend (I) resulted in higher values for hardness and elastic modulus, giving a result of 191.6±10.49 GPa as compared to 167.81±26.10 GPa measure in blend (II).

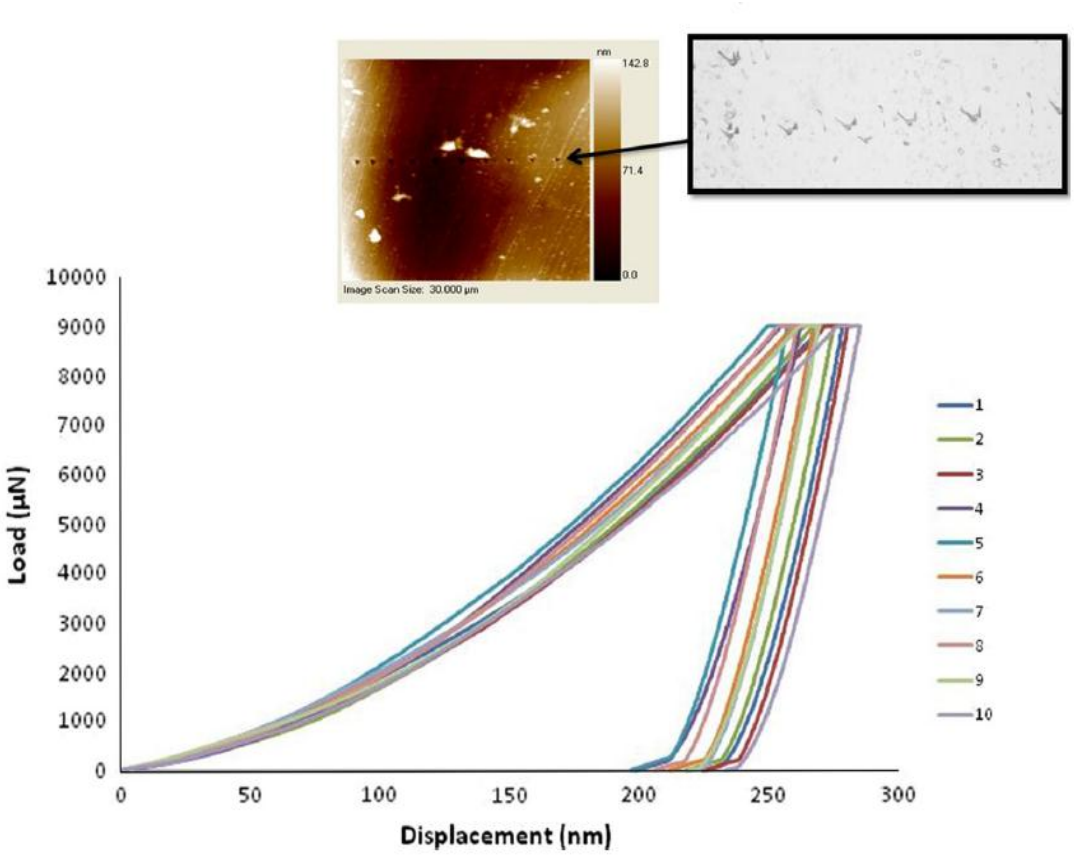

Figure 4.10. Load-displacement diagram of cold sprayed Ni-Ni_3Al < 45 µm (Blend I). The inset is series of nano-indents on the same cold sprayed sample.

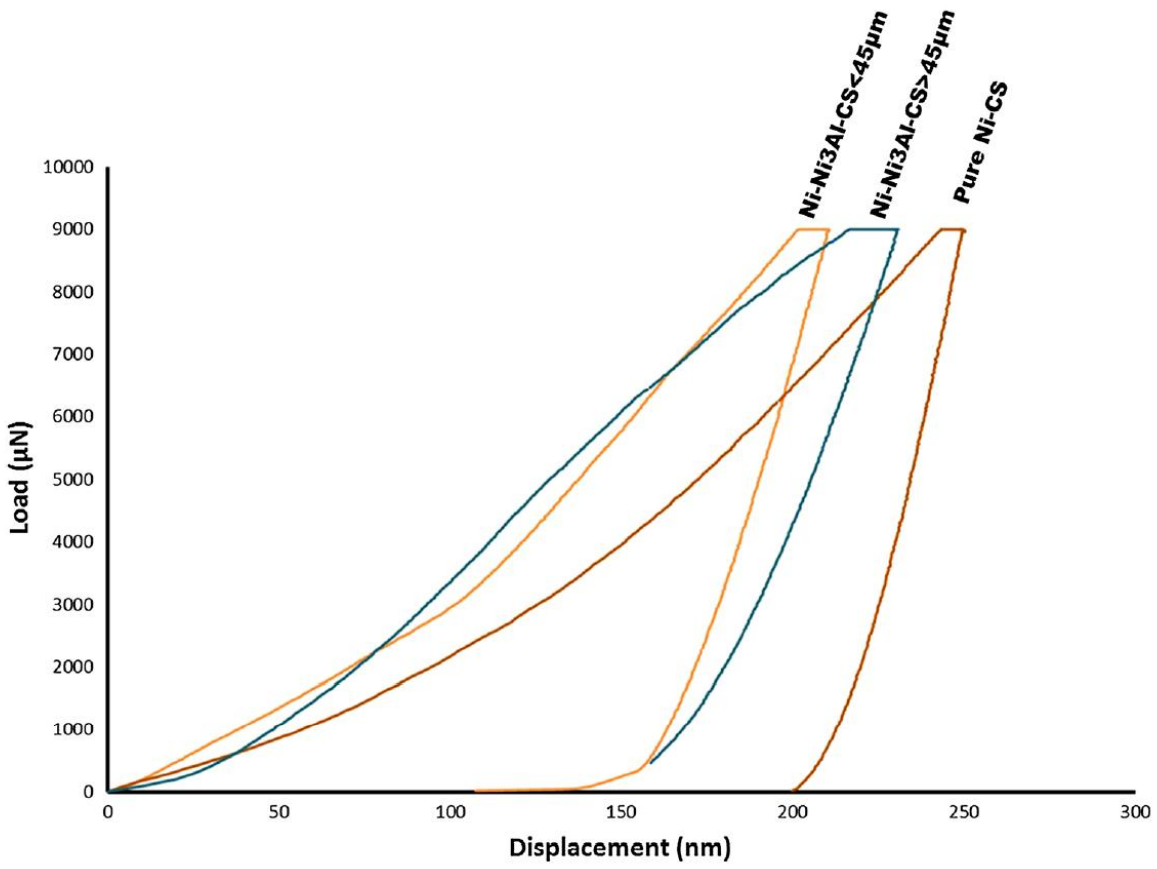

Figure 4.11. Average load-displacement diagram of cold sprayed Blend I, Blend II, and pure Nickel.

Resonant frequency analysis test provided an elastic modulus resulting in minimum deviation as compared to the elastic modulus set by other tests, indicating a certainty in measurements gained using this method. The elastic modulus result for blend (I) using RFA was 193.2±0.4GPa and 160.25 ±0.02 GPa for blend (II). These results make RFA the most accurate choice in obtaining elastic modulus of cold spray coatings.

A summary of the results from Knoop Indentation, Vickers hardness, nano-indentation and RFA for blend (I) and blend (II) is given in Table 4.11. The elastic modulus results from RFA and nano-indentation can be considered fairly well, however this is not true with Knoop

indentation methods showing 27% discrepancies in comparison to the other two methods. Regardless of particle size, the elastic modulus calculated by rule of mixtures provided 195 GPa for Ni-Ni_3Al composites. Few studies conducted by other researchers indicate that the elastic modulus of MMC coatings fabricated using Ni and NiAl were around 180-200 GPa **[8][13]**.

The main objective of this study was to understand the effect of the reinforcement particle size (Ni_3Al) on the mechanical properties of the cold sprayed composite material. Therefore, the results obtained from this study indicates decreasing particle size leads to an increase in elastic modulus and hardness values for cold sprayed coatings. Test data showed cold sprayed MMC manufactured with the Ni_3Al particle size less than 45µm to have 12% higher elastic modulus as compared to the cold sprayed samples manufactured with Ni_3Al particles larger than 45µm. Similar pattern of logarithmic reduction in mechanical properties with increasing particle size for Al based MMCs has been previously studied Prasad et al. (2002) **[55]**. Mechanical properties of Al based MMCs were believed to improve with decreasing reinforcement particle size **[55]**. Another study on the effect of particle size on the microstructure and properties of nickel coatings deposited by kinetic spray mentions that hardness of fabricated coatings would decrease with increasing particle size **[60]**. Considering the results goatherd from current study illustrates that smaller reinforcement particle sizes displayed to be the best fit for cold sprayed MMCs.

Table 4.11. Comparison between obtained results from all experimental tests in this study.

	E/ Nano Indentation (GPa)	E/ Knoop test (GPa)	E / RFA (GPa)	Vickers Hardness (HV)	Knoop Hardness (HK)
Blend I	191.6± 10.49	152.18± 10.1	193.2± 0.4	427.5± 8.2	398.4± 17
Blend II	167.81± 26.10	138.5± 14.5	160.25± 0.02	422.5± 14.36	370.2± 5.2

The bonding strength of a sprayed coating is a contributing factor for the mechanical properties. Previous research has indicated that residual stress within the coating structure, diffusion of particles across the splat boundaries, forces at the atomic level and mechanical interlocking can all be affecting the bonding strength between consecutive splats **[55]**. As shown in Equation 4.3, by the inverse relationship between diameter of the particles and drag force, smaller particles carry higher velocity compared to larger particles that carry lower velocity **[59]**. Although the larger particles carry high kinetic energy at impact, the drag forces at higher velocities for smaller particle work beyond the deposition efficiency at higher rates. This condition can be valid, the particles need to have constant diameter and with perfect spherical shape.

$$D = \frac{1}{2}\rho V_{rel}^2 A_p C_D \qquad \text{(Eq.4.3)}$$

Where D is the drag force acting on the particles, C_D is drag force coefficient, V_{rel} is relative velocity of the particle relative to the gases, and A_p is the surface area of the particle projected.

A research by Assadi et al (2011) observed the effect of sprayed particle velocity on flattening ratio and deposition efficiency and cohesive strength of cold sprayed copper **[72]**. This study concluded that smaller particle resulted in higher velocities for sprayed particle similar to conclusions from some other studies. Assadi et al (2011) introduce two equation in their study to represent the deposition efficiency (Equation 4.4) and cohesive strength (Equation 4.5) in terms of particle size and velocity [**72**]. The equations are,

$$DE = \int_0^\infty gf(d_p)\,\mathrm{d}d_p \qquad \text{(Eq. 4.4)}$$

$$\sigma_c = \sigma_u \left(f\frac{v_{pi}}{v_{cr}} - 1\right) \qquad \text{(Eq. 4.5)}$$

Where g is a function dependent on the size, $\mathrm{d}d_p$ is the differential of particle diameter (d_p), σ_c is coating cohesive strength and σ_u the tensile strength of the coating material. v_{pi} is a particle velocity and v_{cr} is the critical impact velocity which can be define in terms of materials properties.

The higher velocities affect bond strength and deposition efficiency which could be a good explanation as to why blend (I) consisting of smaller particles show better mechanical properties. Some studies have also indicated that higher rates of work hardening during spraying and impact could also result in higher mechanical strength in cold sprayed MMCs with smaller particle sizes **[57]**. Parameters such as gas temperature and particle velocity on the localized substrate temperature and deposition efficiency are previously reported to be resulting in changes in deposition efficiency **[8][75][76]**. However, variation in deposition velocity which changes the particles kinetic energy does not seem to have a significant impact on the substrate temperature

[34][77]. Therefore to eliminate the effect of gas temperature on the substrate temperature and consequent properties of the coatings, the process temperature has been kept constant for this study.

CHAPTER 5. CONCLUSION

This research was mainly intended to show the effectiveness of cold spraying technique as a near net shape forming technique to fabricate MMCs. Secondary objectives were setup to peruse the main objective. The fabricated cold sprayed MMCs were compared to P/M MMCs and pure cold sprayed samples.

One of the secondary objectives was to compare the mechanical and microstructural properties of cold sprayed and P/M samples. Both P/M and cold sprayed Ni-Ni_3Al samples were subjected to multiple experimental tests to determine its hardness and elastic moduli. The cold sprayed sample exhibited higher strength compared to the P/M processed ones. The results from this study indicated that the mechanical interlock in cold sprayed samples was stronger than the combination of weak mechanical and metallurgical bonding in P/M processed samples. It's known that mechanical bonding will occur in cold spraying causing adhesion between the splats and the adjacent coating layers. Unlike in cold spray; P/M uses combination of mechanical bonding during cold and hot pressing stages and metallurgical bonding during hot pressing and sintering steps.

One of the other objectives of this study was to investigate the effect of reinforcement particle size on the mechanical and microstructural properties on the fabricated MMC using cold spraying method. Two different types of blends were used to fabricate samples, where blend (I) contained smaller Ni_3Al particles mixed with Ni and blend (II) contained larger Ni_3Al particles mixed with Ni. Based on the microstructural studies conducted on these samples, there is no solid evidence to prove any major effect of particle size variation on porosity and particle distribution. Mechanical testing on the samples indicated that the MMC cold sprayed sample

made from blend (I) has higher elastic modulus compared to the samples fabricated from blend (II). Both hardness and elastic modulus were decreased with increasing particle size. This phenomenon could be explained due to smaller particles having higher velocity compared to larger particles which resulted in a higher mechanical interlock and increase in adhesion between coating layers.

The effect of adding reinforcement to Ni was also examined in this study. The strengthening process in composites could be attributed to the solid solution strengthening, work hardening, precipitation hardening, and grain boundary strengthening, etc. It was speculated that adding Ni_3Al in to Ni matrix enhanced the mechanical properties of the MMCs. Hence, pure Ni samples were used to fabricate both cold spraying and P/M methods then the obtained results in this study proved the strengthening of Ni material with the addition of Ni_3Al particles. The results obtained from the cold sprayed samples using resonant frequency test and, Marshal equation illustrated that slightly higher elastic moduli was observed in reinforced cold sprayed samples compared to pure cold sprayed ones. The results from Marshal's equation and nano-indentaion indicated that the addition of Ni_3Al reinforcements was more effective in improving the elastic modulus of Ni in P/M processed samples. This study indicated that the addition of 20 vol. % Ni_3Al particles had a slight effect on improvement of the mechanical strength in the P/M processed and cold spraying samples. However further investigation is necessary at different percentages of the reinforcement phase to better understand the effectiveness of Ni_3Al on mechanical properties of P/M and cold spray processed samples.

In conclusion the cold sprayed samples showed better mechanical and microstructural properties compared to P/M samples. Having denser microstructure with lower voids and strong

mechanical bonding proved that the cold spraying technique is a suitable method for near net shape forming of metals and metal matrix composites.

REFERENCE

1. J.R.Davis, Nickel, Cobalt and their alloys, ASM Handbook, 2000.
2. T.Pollock, "Nickel-Based Superalloys for Advanced Turbine Engines: Chemistry, Microstructure, and Properties," Journal of Propulsion and Power, vol. 22, no. 2, pp. 456-466, 2006.
3. P. C. Angelo and R.Subramania, Powder metallurgy: science, technology and applications, PHI Learning, 2008.
4. F. Azarmi and V. J. Gelling, "Corrosion Behavior of Air Plasma Sprayed Alloy 625 on Nickel Foam Substrate," in 2011 International Annual Corrosion Conference and Exposition (NACE),, Houston, TX, 2011.
5. H. P. Xu, A. H. Ngan, B. J. Guggan and Q. Z. Chen, "Toughening of γ'- Ni3Al by γ precipitation," Materials letters, vol. 31, pp. 228-233, 1997.
6. V. M. Kevorkian, "Commercial Viability of Al-Based MMCs in the Automotive Segment," Materials Manufacturing Process, vol. 14, pp. 639-645, 1999.
7. R. Everett, "Deposition technologies for MMC fabrication," in Metal matrix composites: Processing and Interfaces, Elsevier Inc., 1991, pp. 103-118.
8. J.R. Davis , "Cold Spray Process," in Handbook of Thermal Spray Technology, ASM International, 2004, pp. 77-84.
9. T. Steenkiste , J. R. Smith and R. E. Teets, "Aluminum coatings via Kinetic Spray with Relatively large powders Particles," Surface and Coatings Technology, vol. 154, no. 2-3, pp. 237-252, 2002.
10. J. Karthikeyan, "Cold spray technology:International status and USA efforts," ASB Industries, Barberton, OH, 2004.

11. D. Grasme, "Cold Sprayed Verax Heat Sinks," OBZ Grasme & Dresel GmbH Bad Krozingen, Germany, 2003.
12. D. Coutsouradis, J. H. Davidson, J. Ewald, P. Greenfield, T. Khan and D. B. Meadowcroft, "Materials for Advanced Power Engineering," in Kluwer Academic, Liège, Belgium, 1994.
13. T. Goyal and R. S. Walia, "Cold sprayed copper coatings on ASTM B 221 alloy – characterisation and corrosion study in simulated marine and industrial environment," International Journal of Surface Science and Engineering, vol. 10, pp. 1504-1520, 2012.
14. J. Bell, A. Warner and T. F. Stephenson, "Some automotive applications for cast graphitic aluminum nickel silicon carbide MMC," Minerals, Metals & Materials Society, vol. 18, pp. 247-256, 1996.
15. L. Pawlowski, The Science and Engineering of Thermal Spray Coatings, USA: Wiley, 2008.
16. J. C. Williams and E. A. Starke, "Progress in structural materials for aerospace systems," Acta Materialia, vol. 51, pp. 5775-5799, 2003.
17. R. Schafrik and R. Sprague,, "Saga of Gas Turbine Materials: Part III," Advanced Materials and Processes, vol. 162, pp. 27-30, 2004.
18. J. Karthikeyan, "Development of Oxidation Resistant Coatings on GRCop-84 substrates by Cold Sprays Process," ASB Industries, Barberton,OH, 2007.
19. R. C. Redd, The supperalloys: Fundamentals and Applications, Cambridge: Cambridhe University Press, 2006.
20. F. Nabarro and M. S. Duesbery, Diclocations in Solids :L12 Ordered Alloys, Elsevier, 1996.

21. R. Davis, "Phase Diagrams of Binary Nickel Alloys," in Introduction to Aluminum and Aluminum Alloys, ASM International, 1993, pp. 95-125.
22. S. A. Sajjadi, H. R. Elahifar and H. Farhangi, "Effects of cooling rate on the microstructure and mechanical properties of the Ni-base superalloy UDIMET 500," Journal of Alloys and Compounds, vol. 455, pp. 215-220, 2008.
23. J. Maoa, K. Minn and W. Yang, "Cooling precipitation and strengthening study in powder metallurgy superalloy Rene88DT," Materials Science and Engineering, vol. 332, no. A, pp. 318-329, 2002.
24. A. Papyrin, V. Kosarev, A. Klinkov and V. Formin, Cold Spray Technology,, Amsterdam: Elsevier, 2007.
25. J. Villafuerte, "Current and Future Applications of Cold Spray Technology," metalfinishing, Ontario, 2010.
26. P. Fauchais and A. Vardelle, "Thermal Sprayed Coatings Used Against Corrosion and Corrosive Wear," in Advanced Plasma Spray Applications, France, InTech , 2012, pp. 4-37.
27. C. Li, W. Li and H. Liao, "Examination of the Critical Velocity for Deposition of particles in Cold Spraying," Journal of Thermal Spray Technology, vol. 15, pp. 212-222, 2006.
28. S. E. Tinashe, Conceptual Design of a Low Pressure Cold Gas Dynamic Spray (LPCGDS) System, Johannesburg: University of the Witwatersrand, 2010.
29. O. Stier, "Fundamental Cost Analysis of Cold Spray," Journal of Thermal Spray Technology, vol. 23, no. 1-2, pp. 131-139, 2004.

30. R. Ghelichi and M. Guagliano , "Coating by the Cold Spray Process: a state of the art," Frattura ed Integrità Struttural, vol. 8, pp. 30-44, 2009.
31. E. Irissou, J.-G. Legoux and C. Moreau, "Investigation of Al-Al2O3 Cold Spray Coating Formation and Properties," Journal of Thermal Spray Technology, vol. 16, no. 5-6, pp. 661-668, 2007.
32. W.-Y. Li and W. Gao, "Some aspects on 3D numerical modeling of high velocity impact of particles in cold spraying by explicit finite element analysis," Applied Surface Science, vol. 255, no. 18, pp. 7878-7892, 2009.
33. T. Stenkiste, J. Smith, R. Teets and J. Moleski, "Kinetic SoraySpray Coating," Suface and Coatings Technology, vol. 6, pp. 576-582, 1998.
34. D. L. Gilmore, R. C. Dykhuizen, R. A. Neiser, M. F. Smith and T. J. Roemer, "Particle velocity and deposition efficiency in the cold spray process," Journal of Thermal Spray Technology, vol. 8, no. 4, pp. 576-582, 1999.
35. R. C. Dykhuizen and M. F. Smith, "Gas dynamic principles of cold spray," Journal of Thermal Spray Technology, vol. 7, no. 2, pp. 205-212, 1998.
36. M. Karimi, A. Fartaj and G. Rankin, "Numerical Simulation of the Cold Gas Dynamic Spray Process," Journal of Thermal Spray Technology, vol. 15, no. 4, pp. 518-524, 2006.
37. V. K. Champagne, D. Helfritch, P. Leyman, S. Grendahl and B. Klotz, "Interface Material Mixing Formed by the Deposition of Copper on Aluminum by Means of the Cold Spray Process," Journal of Thermal Spray Technology, vol. 14, no. 3, pp. 330-334, 2005.

38. R. M. German, Powder Metallurgy and Particulate Materals Processing: The Processes, Materials, Products, Properties and Applications, Metal Powder Industries Federation, 2005.
39. G. Dowson, Powder metallurgy: the process and its products, A. Hilger, 1990.
40. W. A. Kaysser, "Solid State Sintering," in Powder Metallurgy - An Overview, London, The Institute of Metals, 1991, pp. 168-182.
41. W. Schatt and K.-P. Wieters, Powder Metallurgy - Processing and Materials, European Powder Metallurgy Association, 1997.
42. E. N. G. Gregolin, R. G. d. Santos and H. Goldenstein, "Application of Powder Metallurgy to Obtain Al/SiO2 Composites," Key Engineering Materials, Vols. 189-191, pp. 529-534, 2001.
43. D. Sharma, K. Chandra and P. S. Misra, "Design and development of powder processed Fe–P based alloys," Materials & Design, vol. 32, no. 6, pp. 3198-3204, 2011.
44. V. S. Warke, R. D. Sisson Jr. and M. M. Makhlouf, "The effect of porosity on the austenite to ferrite transformation in powder metallurgy steels," Materials Science and Engineering: A, vol. 528, no. 10-11, pp. 3533-3538, 2011.
45. H. D. Solomon and L. F. Coffin Jr., "Effects of frequency and environment on fatigue crack growth in A286 at 1100 oF," in Fatigue at Elevated Temperature,ASTM STP 520, Philadelphia,, American Society for Testing and Materials, 1973, pp. 112-114.
46. L. A. James, "Some Questions Regarding the Interaction of Creep and Fatigue," Journal of Engineering Materials and Technology, vol. 98, no. 3, pp. 235-243, 1975.

47. H. Yang, R. Bao, J. Zhang, L. Peng and B. Fei, "Crack growth behaviour of a nickel-based powder metallurgy superalloyunder elevated temperature," International Journal of Fatigue, vol. 33, pp. 632-641, 2011.
48. K. C. Kerider, Metallic Matrix Composite, New York: Academic Press, 1974.
49. K. Chawla, Composite Materials: Science & Engineering (2), New York: Springer-Verlag, 199.
50. Y. B. Liu, S. C. Lim, L. Lu and M. O. Lai, "Recent development in the fabrication of metal matrix-particulate composites using powder metallurgy techniques," Journal of Materials Science, vol. 29, no. 9, pp. 1999-2007, 1994.
51. P. Vincenzini, Ed., Ceramics today--tomorrow's ceramics: proceedings of the 7th International Meeting on Modern Ceramics Technologies (7th CIMTEC--World Ceramics Congress), Montecatini Terme, Italy: Elsevier, 1991.
52. P. L. Rathaparkhi and H. J. Rack, "Aging effects on the fracture toughness of SiC whisker reinforced 2XXX aluminum alloys," Advanced Materials and Manufacturing Processes, vol. 23, pp. 2143-2146, 1989.
53. A. Geiger and J. Walker, "The processing and properties of discontinuously reinforced aluminum composites," Journal of Metals, vol. 43, pp. 8-15, 1991.
54. I. C. Stone and P. Tsakiropoulous, "Characterisation of spatial distribution of reinforcement in powder metallurgy route Al/SiCp metal matrix composites," Material Scinece Engineering, vol. A, no. 189, pp. 213-221, 1995.
55. V. Prasad , B. V. Bhat, Y. Mahajan and P. Ramakrishnan, "Structure–property correlation in discontinuously reinforced aluminium matrix composites as a function of relative particle size ratio,," Material Science Engineering, vol. A, no. 337, pp. 179-184, 2002.

56. J. J. Lewandowski, Intrinsic and Extrinsic Fracture Mechanisms in Inorganic Composite Systems: Proceedings of a Symposium Sponsored by the Structural Materials Divisio, W. H. Hunt Jr. , Ed., Warrendale,PA: TMS, 1995.

57. W. H. Hunt , T. Osman and J. J. Lewandowski, "Structure-Property Relations in Discontinuously Reinforced Aluminum (DRA) Alloys," Journal of materials, vol. 45, pp. 30-35, 1993.

58. H. N. Yoshimura, M. C. Gonçalves and H. Goldenstein, "The Effects of SiCp Clusters and Porosity on the Mechanical Properties of PM Al Matrix Composites," Key Engineering Materials, Vols. 127-131, pp. 985-992, 1996.

59. B. Jodoin, L. Ajdelsztanjn, E. Sansoucy, A. Zuniga and P. Richer, "Effect of particle size, morphology, and hardness on cold gas dynamic sprayed aluminum alloy coatings," Sufrace & Coatings Technology, vol. 201, pp. 3422-3429, 2006.

60. G. Bae, K. Kang, J. Kim and C. Lee, "Effect of particle size on the microstructure and properties of kinetic sprayed nickel coatings," Surface & Coatings Technology, vol. 204, pp. 3326-3335, 2010.

61. H. Koivuluoto, G. Bolelli, A. Milantia, L. Lusvarghib and P. Vuoristo, "Microstructural analysis of high-pressure cold-sprayed Ni, NiCu and NiCu + Al2O3 coatings," Surface and Coatings Technology, vol. 268, pp. 224-229, 2015.

62. G. Yang and C. Li, "Effect of heat treatment on the microstructure and property of cold-sprayed nanostructured FeAl/Al2O3 intermetallic composite coating," Vacuum, vol. 83, no. 1, pp. 146-152, 2008.

63. "ASTM Standard: A370 Test Methods and Definitions for Mechanical Testing of Steel Products," in Annual Book of ASTM Standards Vol. 01.04., 1980.

64. K. Zeng, "Nanoindentation of thin films and its applications,," in Handbook of nanoceramics and their based nanodevices, American Scientific Publishers, 2009, pp. 175-205.

65. A. Fisher-Cripps, Nanoindentation: Second edition, New York: Springer, 2004.

66. T. Powers, "Measuring Young's Modulus of Elasticity by Means of Sonic Vibrations," in ASTM Proceeding - Volume 38, 1938.

67. J. Rayleigh, Theory of Sound (2nd edition), New York: Dover Press, 1945.

68. "ASTM C 215-85," Annual Book of ASTM Standards, vol. 04, no. 02, pp. 123-135, 1986.

69. M. Bashirzadesh, F. Azarmi, C. Leither and G. Karami, "Investigation on Relationship Between Mechanical Properties and Microstructural Characteristic of Metal Matrix Composites Fabricated by Cold Spraying Technique," Applied Surface Science, vol. 275, pp. 208-216, 2014.

70. V. Steenkiste and J. R. Smith, "Evaluation of coatings produced via kinetic and cold spray processes," Journal of Thermal Spray Technology, vol. 13, no. 2, pp. 274-282, 2004.

71. S. H. Zahiri, D. Fraser, S. Gulizia and M. Jahedi, "Effect of processing conditions on porosity formation in cold gas dynamic spraying of Copper," Journal of Thermal Spray Technology, vol. 15, no. 3, pp. 422-430, 2006.

72. H. Assadi, T. Schmidt, H. Richter, J. O. Kliemann, K. Blinder, T. Klassen and H. Kreye, "On Parameter Selection in Cold Spraying, Therm. Spray Technol. ,," Journal of Thermal Spray Technology, vol. 20, no. 6, pp. 1165-1181, 2011.

73. D. B. Marshal, T. Noma and A. Evans, "A Simple method to determining elastic modulus-to-hardness ratio using Knoop indentation mesurements," Journal of American Ceramic Society, vol. 65, pp. 175-178, 1982.
74. T. Stoltenhoff, H. Kreye and H. J. Richter, "An analysis of the cold spray process and its coatings," Journal of Thermal Spray Technology, vol. 11, no. 4, pp. 542-550, 2002.
75. J. G. Legoux, E. Irissou and C. Moreau, "Effect of Substrate Temperature on the Formation Mechanism of Cold-Sprayed Aluminum, Zinc and Tin Coatings," Journal of Thermal Spray Technology, vol. 16, no. 5-6, pp. 619-626, 2007.
76. M. Fukumoto , H. Wada, K. Tanabe, M. Yamada and E. Yam, "Effect of Substrate Temperature on Deposition Behavior of Copper Particles on Substrate Surfaces in the Cold Spray Process," Journal of Thermal Spray Technology, vol. 16, no. 5-6, pp. 643-650, 2007.
77. A. Astarita, M. Durante, A. Langella, M. Montuori and A. Squillace, "Mechanical characterization of low-pressure cold-sprayed metal coatings on aluminium," Surface and Interface Analysis, vol. 45, no. 10, pp. 1530-1535, 2013.